

MEASUREMENTS OF THE PARTICLES AND GASES
IN THE GROUND CLOUD FROM AN ATLAS/CENTAUR ROCKET

by

Lawrence F. Radke, Mark W. Eltgroth, Dean A. Hegg and Peter V. Hobbs

Cloud and Aerosol Research Group, Atmospheric Sciences Department
University of Washington, Seattle, Washington 98195

Final Report to the Argonne National Laboratory under Contract No. 37-109-38-4890

February 9, 1979

(All publication and presentation rights reserved by the authors.)

TECHNICAL REPORT STANDARD TITLE PAGE

1. REPORT NO.	2. GOVERNMENT ACCESSION NO.	3. RECIPIENT'S CATALOG NO.	
4. TITLE AND SUBTITLE Measurements of the Particles and Gases in the Ground Cloud from an Atlas/Centaur Rocket		5. REPORT DATE February 9, 1979	6. PERFORMING ORGANIZATION CODE
7. AUTHOR(S) Lawrence F. Radke, Mark W. Eltgroth, Dean A. Hegg and Peter V. Hobbs		8. PERFORMING ORGANIZATION REPORT NO.	
9. PERFORMING ORGANIZATION NAME AND ADDRESS Cloud and Aerosol Research Group Atmospheric Sciences Department, AK-40 University of Washington Seattle, WA 98195		10. WORK UNIT NO.	11. CONTRACT OR GRANT NO. 37-109-38-4890
12. SPONSORING AGENCY NAME AND ADDRESS Argonne National Laboratory Energy and Environmental Systems Division Argonne, IL 60439		13. TYPE OF REPORT AND PERIOD COVERED Final Report November 1978-March 1979	
15. SUPPLEMENTARY NOTES		14. SPONSORING AGENCY CODE	
16. ABSTRACT <p>Fifty-two airborne penetrations have been made of the clouds of materials generated by a night-time launch of an Atlas/Centaur liquid fuel rocket used to launch a satellite from the Kennedy Space Flight Center, Florida. In each penetration detailed measurements were obtained of the particles and gases produced by the rocket.</p> <p>The launch pad cloud and portions of the flame trench cloud were sub-saturated within 3 min of launch. These clouds initially contained mm-sized pieces of launch pad debris in mass concentrations of 1 g per cubic meter of air, however, these large particles were rapidly depleted by sedimentation. The launch pad cloud sank rapidly back down from its maximum height of ~1100 m AGL to near the top of the marine layer at ~700 m AGL.</p> <p>The ground cloud, that was produced near the top of the marine layer by the launch pad cloud combining with the flame trench cloud, was tracked by the aircraft for 135 min as it diffused slowly in the horizontal plane.</p> <p>The concentrations of NO and NO₂ were initially relatively high and the O₃ concentration nearly zero in the ground cloud. The rate of conversion of NO to NO₂ was limited by the rate at which ambient O₃ was mixed into the ground cloud. Methane concentrations in the ground cloud were similar to</p> <p style="text-align: right;">(continued)</p>			
17. KEY WORDS AND DOCUMENT ANALYSIS a. DESCRIPTORS-- Rocket exhaust/ground cloud/pollution/gas-to-particle conversion/cloud condensation nuclei b. IDENTIFIERS-- Cape Canaveral/Kennedy Space Flight Center c. COSATI Field/Group			
18. DISTRIBUTION STATEMENT Available from the National Technical Information Service, Operations Division, Springfield, Virginia 22151.		19. SECURITY CLASS (THIS REPORT) UNCLASSIFIED	21. NO. OF PAGES
		20. SECURITY CLASS (THIS PAGE) UNCLASSIFIED	22. PRICE

ABSTRACT (continued)

those in the ambient air, but up to 49 min after the launch the total non-methane hydrocarbon in the ground cloud were slightly higher than in the ambient air.

The concentrations of particles in the ground cloud were particularly prominent around particle sizes of $5 \times 10^{-3} \mu\text{m}$ and $0.1 \mu\text{m}$. The larger particles were probably due to direct injection from the rocket and the smaller particles to gas-to-particle conversion in the plume. Within 25 min of the launch, most of the mass of the particles in the ground cloud were less than a few micrometers in size. The average density of the particles was 1.1 g m^{-3} . The total mass of particles in the ground cloud remained fairly constant for at least 70 min after launch but it was surprisingly small ($\sim 1 \text{ kg}$, or 0.012% of the propellant that was burned).

TABLE OF CONTENTS

<u>SECTION</u>	<u>PAGE</u>
1. Introduction	1
2. Visual observations	1
3. Liquid water content of the clouds	4
4. Trace gas concentrations, light-scattering coefficients and turbulence in the launch pad and ground clouds	8
5. Particle size distributions in the ground cloud	12
6. Hydrocarbons	22
7. Volumes and emission factor of the ground cloud	26
8. Average density of the particles in the ground cloud	30
9. Trace gas reactions	30
10. Production of cloud condensation nuclei	32
11. Meteorological influences on ambient air samples in the vicinity of Cape Canaveral	33
12. Summary and conclusions	36
Acknowledgments	39
References	39
Appendix A	41
Appendix B	55
Appendix C	62
Appendix D	64

MEASUREMENTS OF THE PARTICLES AND GASES
IN THE GROUND CLOUD FROM AN ATLAS/CENTAUR ROCKET

1. Introduction

This report describes the results of measurements of the particles and gases in the clouds of material generated by an Atlas/Centaur liquid fuel rocket that was used to launch a satellite from the Kennedy Space Flight Center at 0024 EST on November 13, 1978.

The measurements were made aboard the University of Washington's B-23 research aircraft, which is equipped with instruments designed to quantitatively describe the major particle and trace gas emissions expected from a combustion process (see Appendix A for a description of the research aircraft facility). The measurement set consists of 52 penetrations of the materials suspended in the air below ~ 1100 m as a result of the rocket launch. The penetrations were made between 3 and 150 min after the rocket was launched.

2. Visual observations

A schematic of the distribution of materials that were observed^{*} to be suspended in the air as a result of the launch of the Atlas/Centaur rocket is shown in Fig. 1. The principal clouds of material that were observed below ~ 1100 m AGL at $T + 2$ min ($T =$ time of launch) appeared to be (Fig. 1a): a cloud (called the launch pad cloud) that rose vertically from the launch pad to a stable atmospheric layer at ~ 1100 m AGL (Fig. 2), and a cloud that rose at an angle from the trench beneath the launch pad to the top of the marine inversion at ~ 700 m AGL (this is called the flame trench cloud).

* The launch was at night; however, the clouds of materials produced by the rocket initially could be seen in the lights of the launch pad and the B-23 aircraft landing lights.

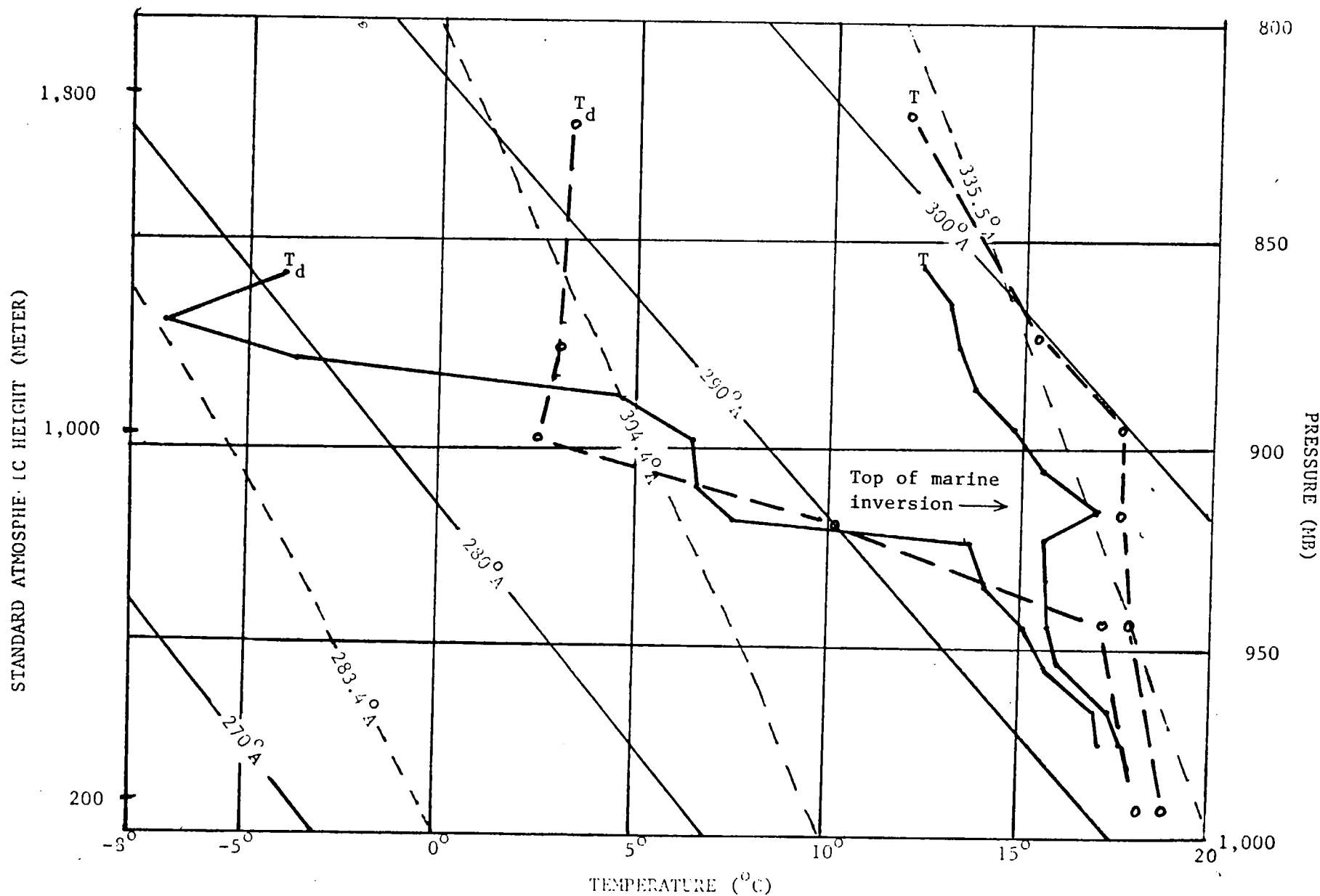
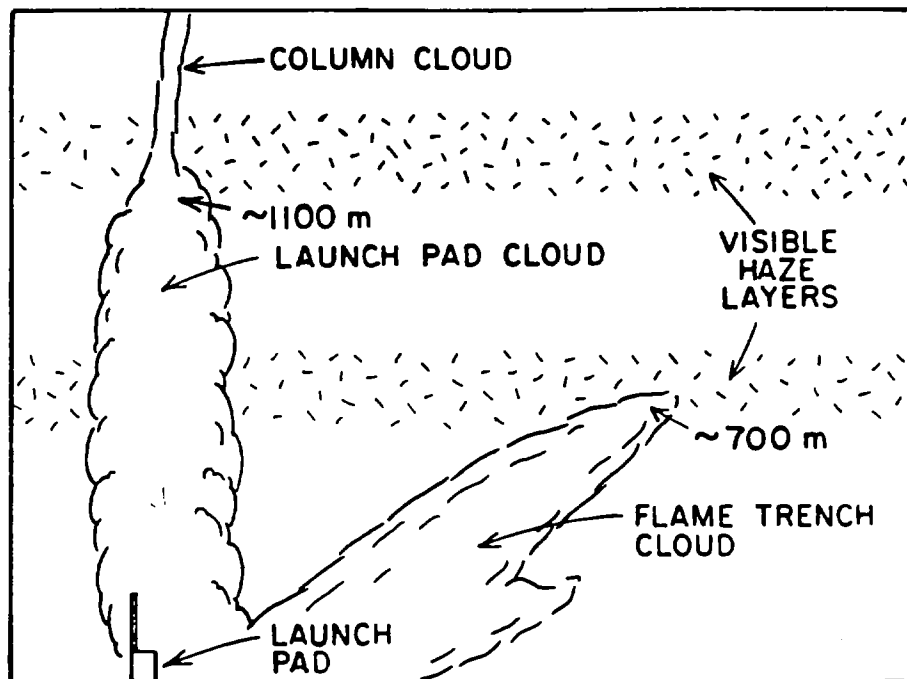
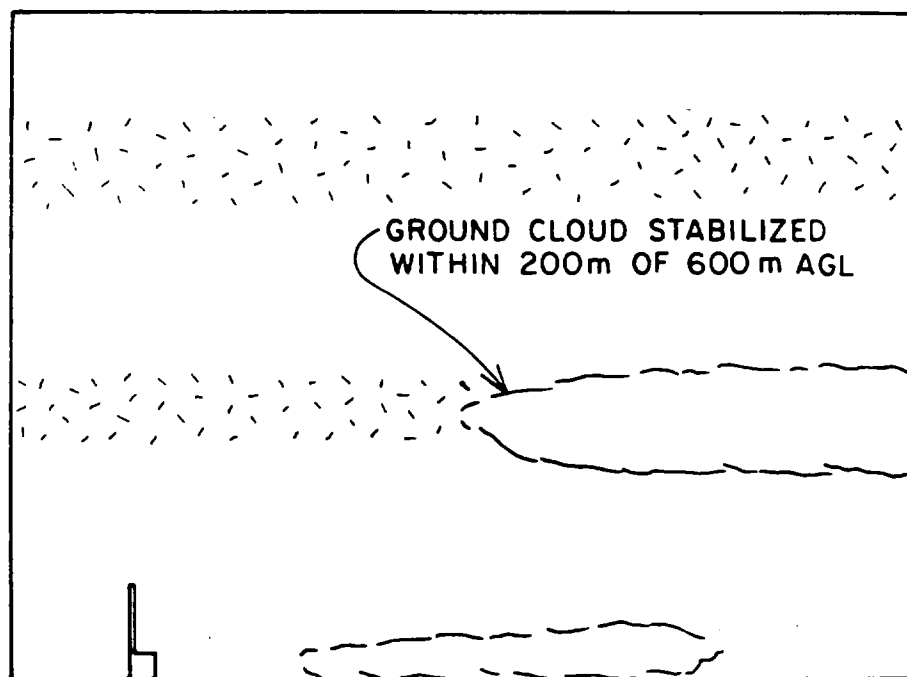


Fig. 2 The aircraft sounding (solid lines) was taken at 00:00 EST November 13, 1978. The Cape Canaveral sounding (dashed lines) was taken at T + 35 min. The sloping solid lines are lines of constant potential temperature. The sloping broken lines are lines of equivalent potential temperature. The differences between the sounding obtained from the aircraft and the radiosonde sounding from Cape Canaveral are presumably due to differences in both time and position.



(a)



(b)

Fig. 1 Schematic of the clouds of material associated with the launch of the Atlas/Centaur rocket based on visual observations from the B-23 research aircraft. (a) About 2 min after launch. (b) About 7 min after launch.

The launch pad cloud was observed to rapidly subside between $T + 2$ min and $T + 15$ min. Subsequently, it probably combined with the flame trench cloud near the top of the marine inversion to form what is referred to as the ground cloud*. At $T + 7$ min the ground cloud was observed drifting slowly westward (Fig. 1b).

3. Liquid water content of the clouds

The first penetration by the B-23 aircraft of the clouds produced by the launch was at $T + 3$ min (0027 EST) at an altitude of ~ 1100 m near the maximum vertical extent of the launch pad cloud. Visual examination of this cloud showed vigorous convection and a definite bluish coloration (indicative of high concentrations of submicron-sized particles). The cloud also appeared translucent rather than opaque as would a cloud of liquid water drops. Moreover, the Johnson-Williams liquid water meter aboard the aircraft showed no signal in excess of noise (0.05 grams of liquid water per cubic meter of air would have given a discernible signal) on any of the penetrations of the cloud. Also, no signs of moisture were observed on the aircraft windscreen.

The temperature/dewpoint spread just prior to penetration was $\sim 14^{\circ}\text{C}$ and at plume center it was $\sim 12.5^{\circ}\text{C}$. At plume center the temperature was $\sim 1^{\circ}\text{C}$ above ambient and the dewpoint $\sim 2.5^{\circ}\text{C}$ above ambient. Since the dewpoint sensor can track a perturbation at a rate greater than 2°C s^{-1} , the aircraft was in the cloud an adequate time to establish that the launch pad cloud was indeed subsaturated with respect to liquid water at $T + 3$ min.

* It is possible that a portion of the launch pad cloud remained above the marine inversion. We have no evidence of this however since all other measurements were confined to the ground cloud once it had formed.

Later penetrations of the launch pad cloud, as it subsided into the moist marine layer to form the ground cloud, showed it to be much closer to water saturation. Thus at T + 6 min the temperature/dewpoint spread was only 1-2°C in the ambient air and 0.5-1°C within the launch pad cloud. However, even in this moist environment, there was no sign of any liquid water.

Despite the lack of liquid water, the launch pad cloud was not devoid of large particles. The particle measuring probes aboard the B-23 aircraft (ASSP, PMS-2, PMS-3) detected significant concentrations of particles as large as 200 μm diameter at T + 5 min in the subsiding of the launch pad cloud (Fig. 3). In the top of what may have been the flame trench cloud, particles as large as 1 mm were found in concentrations of $3 \text{ to } 5 \times 10^{-3} \text{ cm}^{-3}$ at T + 6 min (Fig. 4). Based on the appearance of these particles (Hindman and Grant, 1979) and their high densities (see §8), they appeared to be launch pad debris. The maximum particle mass concentration (calculated from the data shown in Fig. 4 and assuming a particle density of 1 g cm^{-3}) was nearly 1 g m^{-3} . There is no doubt but that if these particles were liquid they would have been detected by the Johnson-Williams liquid water meter*. It should also be noted that such a large mass concentration of particles, while only briefly encountered, is almost certainly damaging to aircraft engines.

The working hypothesis in this report is that while the flame trench and launch pad clouds may have been initially saturated, they quickly entrained dry environmental air so that by the time they combined, the ground cloud was subsaturated.

* Measurements which were obtained in the ground cloud from a Titan solid booster rocket, that was launched from Cape Kennedy on December 13, showed the cloud to be initially saturated and to contain a moderate liquid water content and a high concentration of liquid droplets.

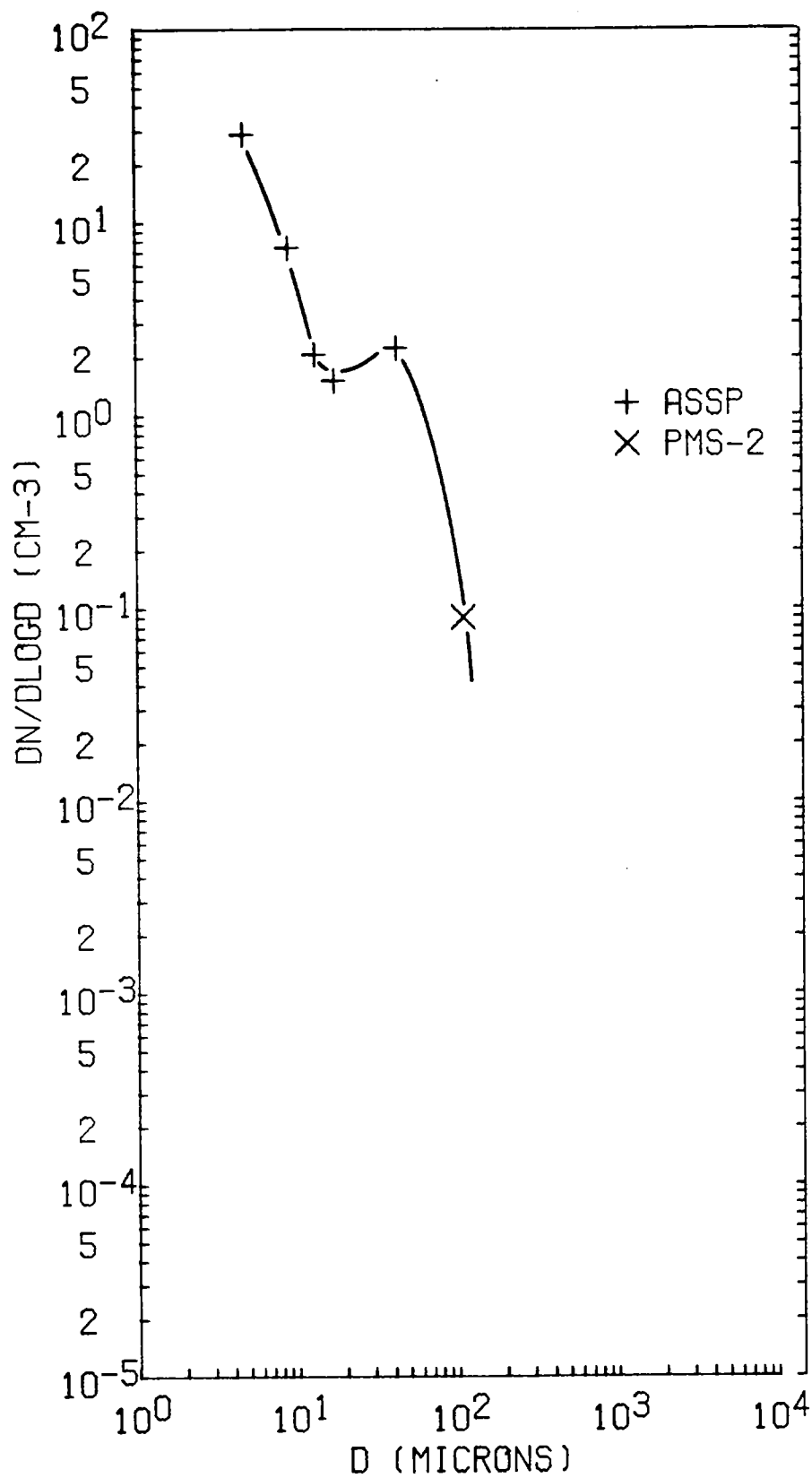


Fig. 3 Point plot of particle number concentration per log size interval $dN/d \log D$ (in units cm^{-3}) versus particle diameter D (in μm) at $T + 5$ min and at 610 m AGL in the subsiding launch pad cloud.

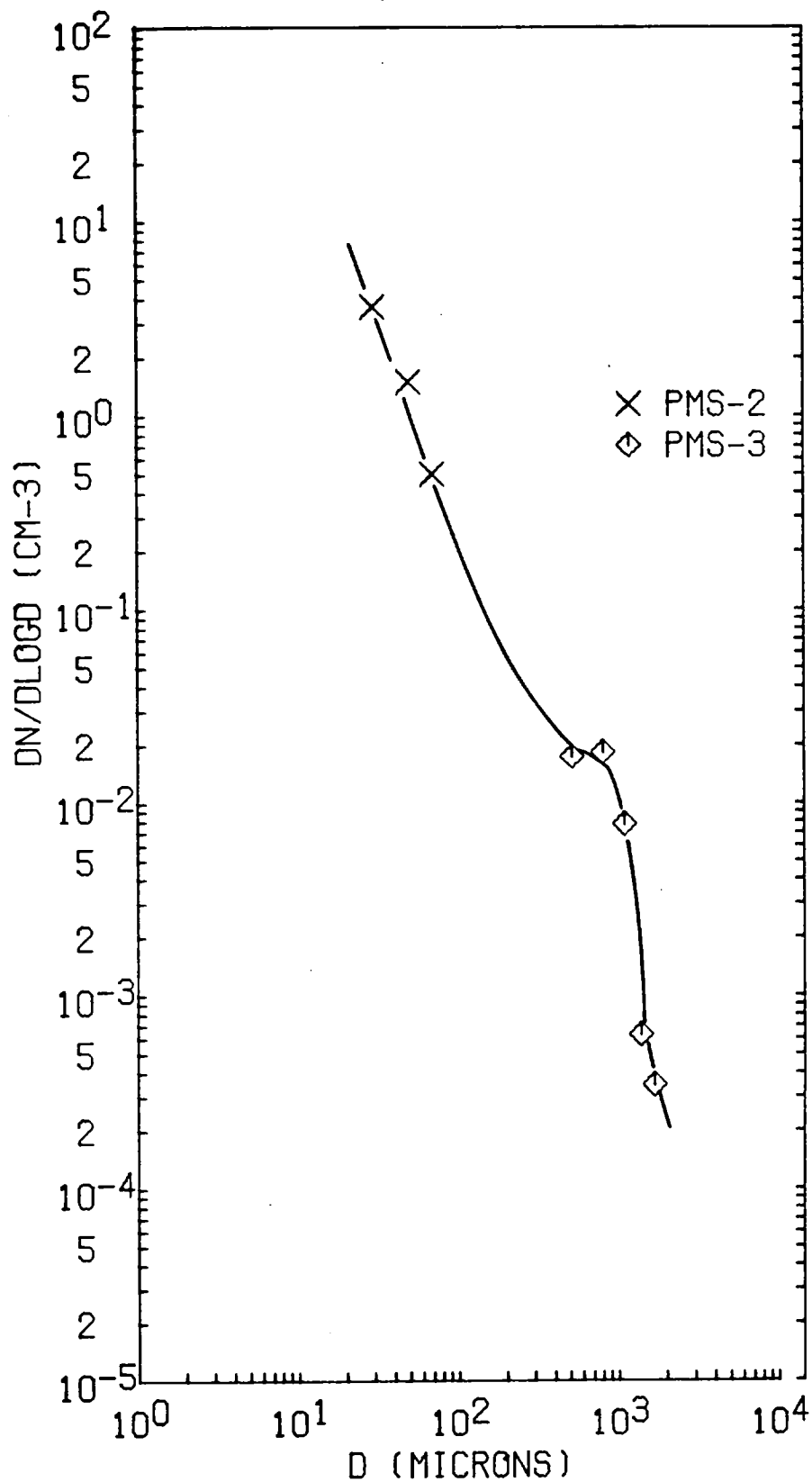


Fig. 4 Point plot of particle number concentration per log size interval $dN/d \log D$ (in units cm^{-3}) versus particle diameter D (in μm) at $T + 6$ min and 610 m AGL altitude in the top of the flame trench cloud.

4. Trace gas concentrations, light-scattering coefficients and turbulence in the launch pad and ground clouds

The characteristics of the ground cloud, as monitored by the continuous gas and particle measuring instruments aboard the B-23 aircraft, were, in many ways, similar to the plume from a thermal power plant fired with low-sulfur coal that has defective pollution-control equipment.

The ground cloud had a distinct SO_2 , NO_2 , NO , O_3 , condensation nucleus (CN), and ion concentration (IC) signatures and less distinct dewpoint, turbulence and vertical electric field signatures.

Using these signatures as real-time detectors, we were able to repeatedly penetrate first the launch pad cloud and then the ground cloud over a period of 147 min even though it was dark and the ground cloud was generally invisible. During this time the ground cloud traveled about 45 km as shown in Fig. 5. Detailed descriptions of the aircraft flight tracks with respect to the clouds were constructed from radar plots and the aircraft navigation system (see Appendix B).

Figure 6 shows some of the measurements obtained in the first six penetrations of the launch pad cloud. The first penetration was very near the top of the launch pad cloud, with most of the cloud passing below the flight level. However, in the subsequent five penetrations a substantial portion of the launch pad cloud was sampled. Notable features of the measurements shown in Fig. 6 are the sharp increases in turbulence, SO_2 , NO and NO_2 concentrations and the light-scattering coefficient as the launch pad cloud was penetrated, and the complete removal of the ambient O_3 . (The small decreases in NO_2 just prior to each penetration of the cloud is an instrument artifact.)

As the launch pad cloud descended to the top of the marine layer and

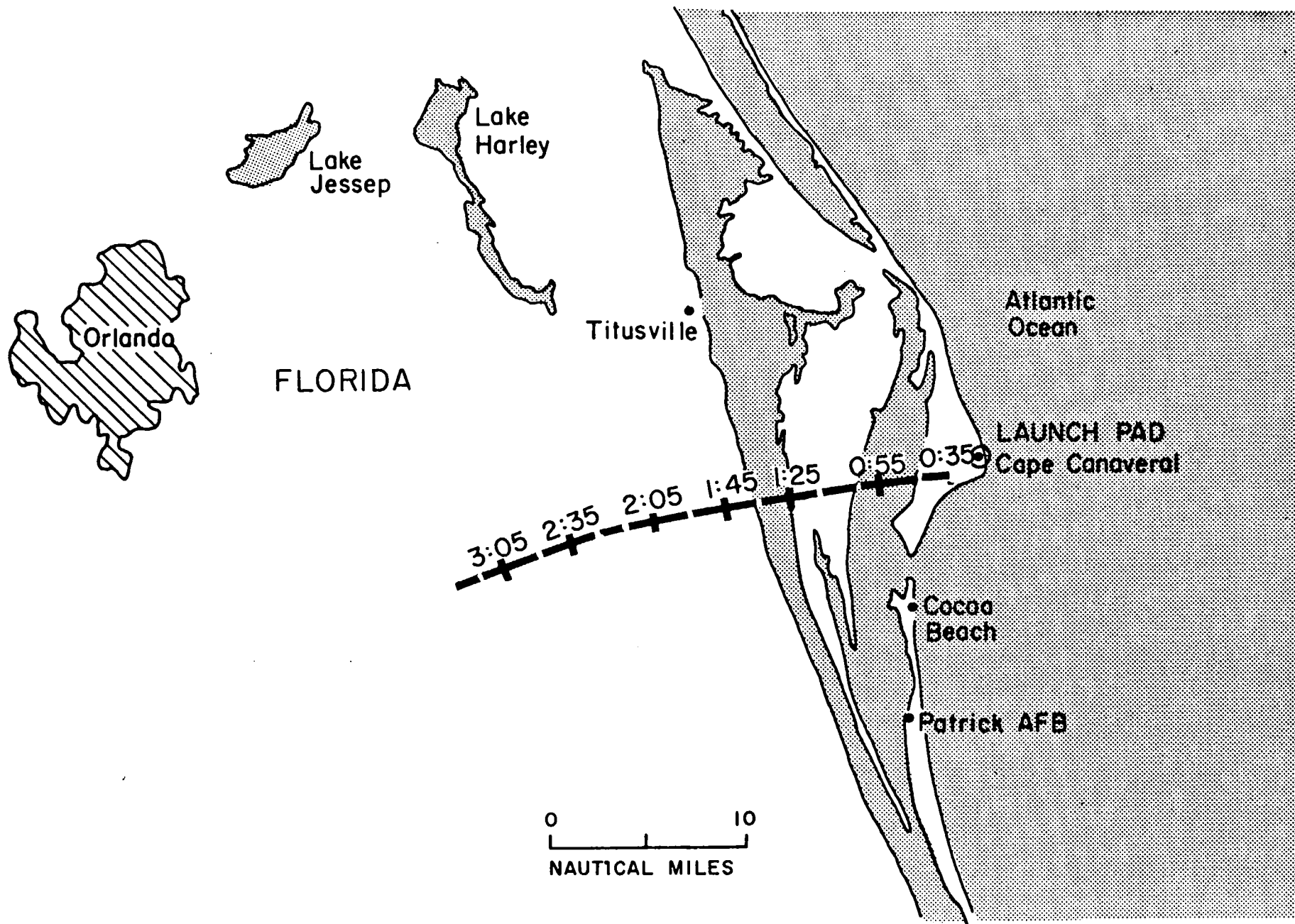


Fig. 5 Track of the ground cloud as it drifted westward from the launch pad at Cape Canaveral. The numbers on the track give the time (hr:min EST).

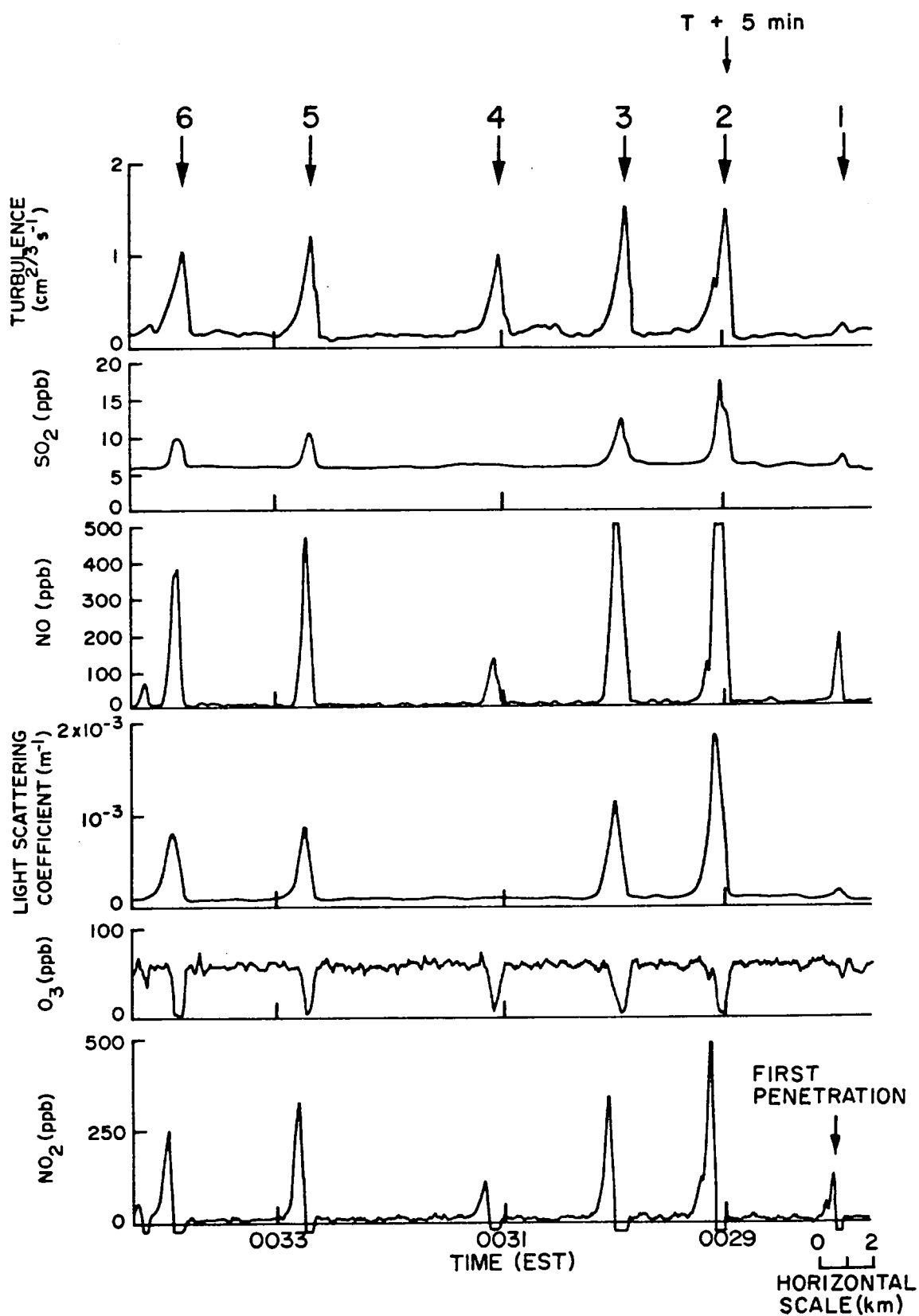


Fig. 6 Some measurements from the initial series of six aircraft penetrations (indicated by arrows at top of diagram) of the launch pad cloud. The first penetration was at 0028 EST near the upper portion of the launch pad cloud. The remaining five penetrations were at lower levels in the launch pad cloud.

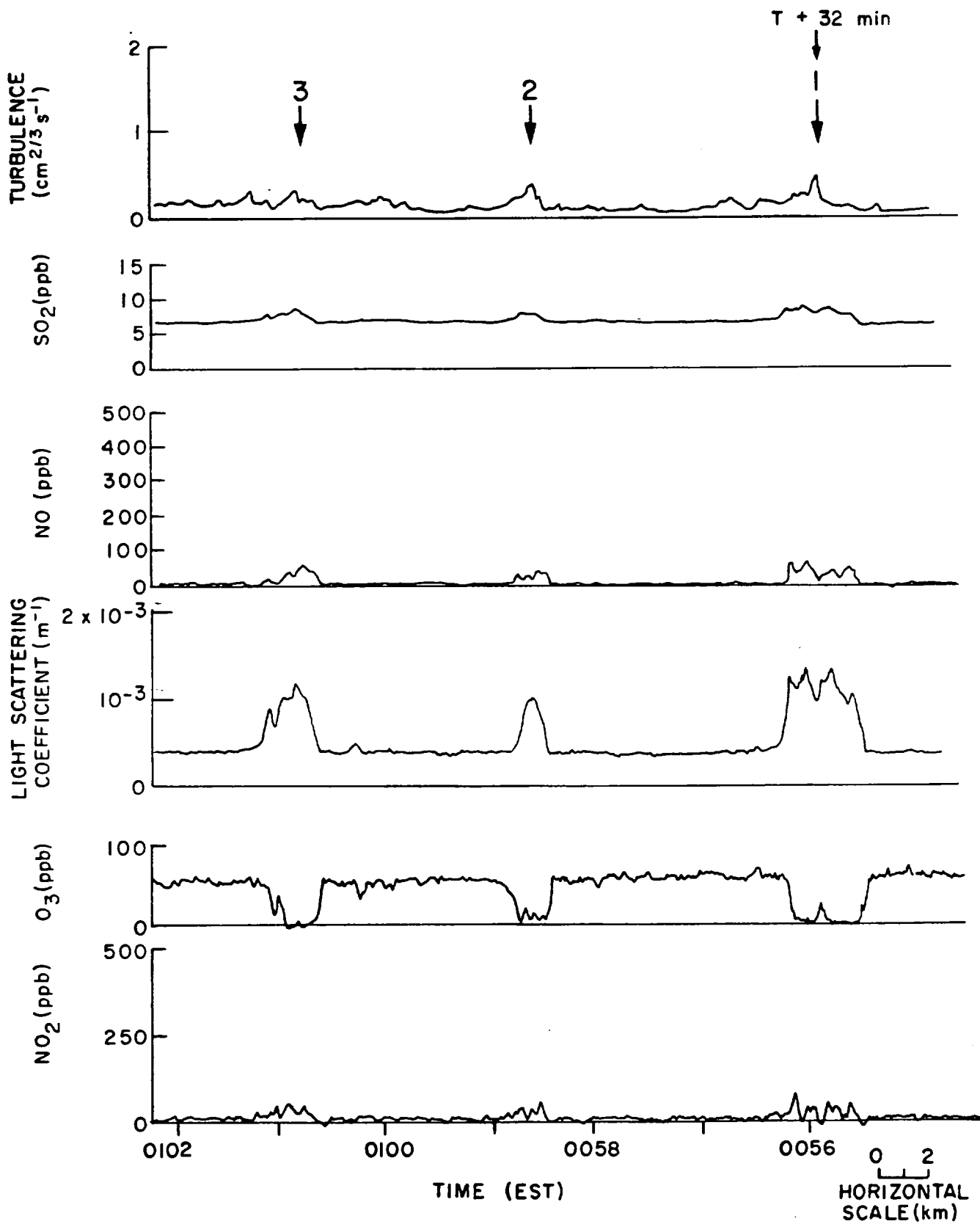


Fig. 7 Measurements obtained in three penetrations (indicated by arrows at top of diagram) of the ground cloud starting 32 min after the launch.

mixed with the flame trench cloud, the combined ground cloud was no longer symmetrical but showed a pronounced major and minor axis. Fig. 7 shows three penetrations of the ground cloud starting at T + 32 min (0056 EST) that were made on nearly orthogonal headings. The measurement at T + 46 min was made along a track that was similarly oriented to the track at T + 32 min, while the track at T + 44 min was made on a heading $\sim 90^\circ$ to the other two. The location of the ground cloud is still quite clear from the measurements shown in Fig. 7. However, in Fig. 7 the turbulence in particular is considerably less in the ground cloud than in Fig. 6.

By T + 89 min the continuously measured variables that clearly defined the ground cloud had decreased to O_3 , NO_2 , NO and the light-scattering coefficient (Fig. 8). By T + 133 min detection had become more difficult (Fig. 9) as the characteristics of the ground cloud approached those of the ambient air. However, the factor which ultimately ended our study was the sharp plume seen at ~ 0239 in Fig. 9. This plume originated from a ground source of combustion that merged with the ground cloud. Since it was difficult to distinguish this plume from the ground cloud, the airborne measurements were terminated at this point.

A complete listing of all the measurements obtained in the ground cloud is given in Appendix C.

5. Particle size distributions in the ground cloud

Particle size distributions in the ground cloud and the ambient air were measured from 28-liter "grab" samples. The "grab" samples in the ground cloud were taken when the continuously measured variables described in §4 showed the aircraft to be near the center of the ground cloud.

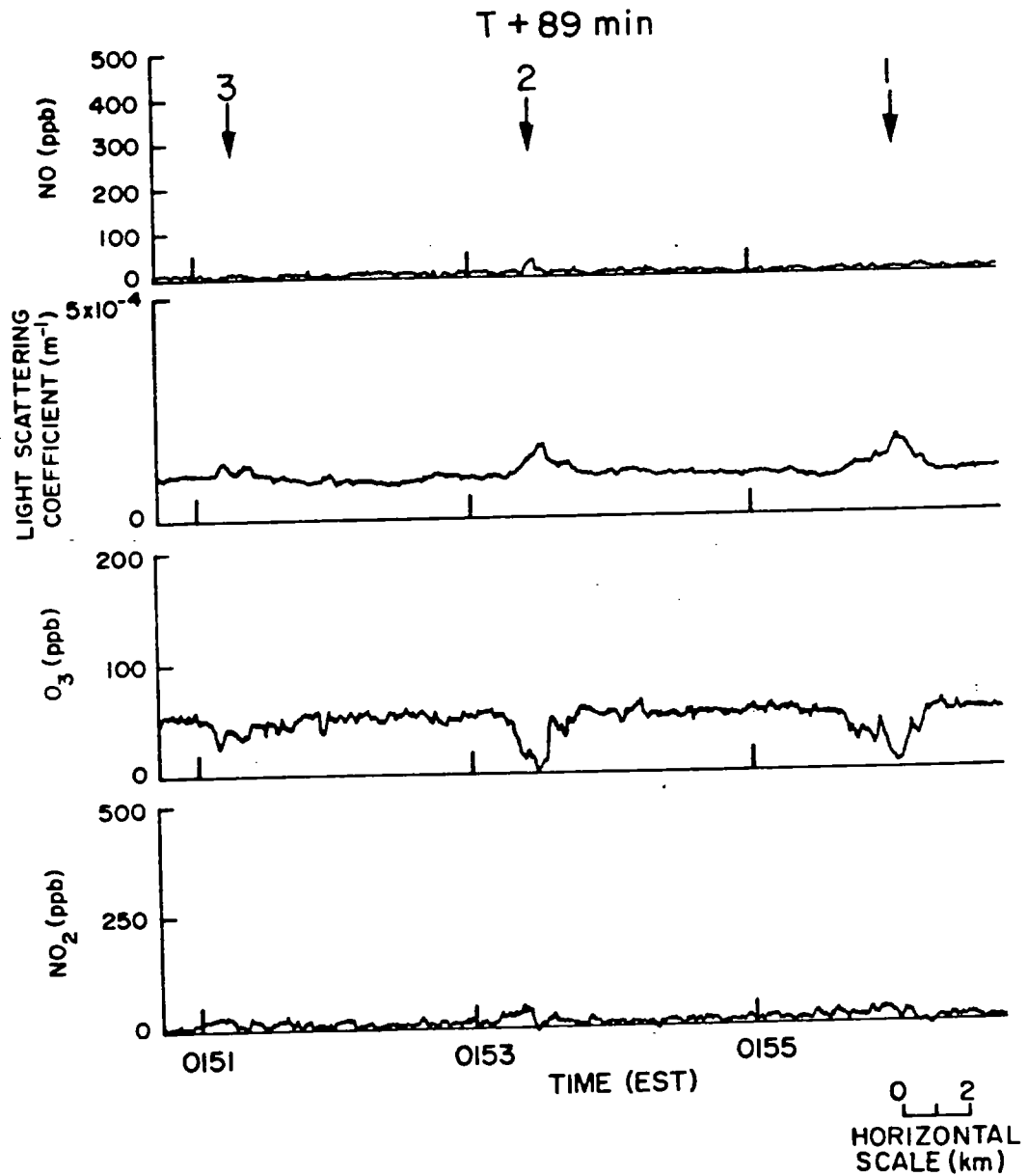


Fig. 8 The continuously measured variables which clearly showed the ground cloud signature around T + 89 min. Three penetrations are shown.

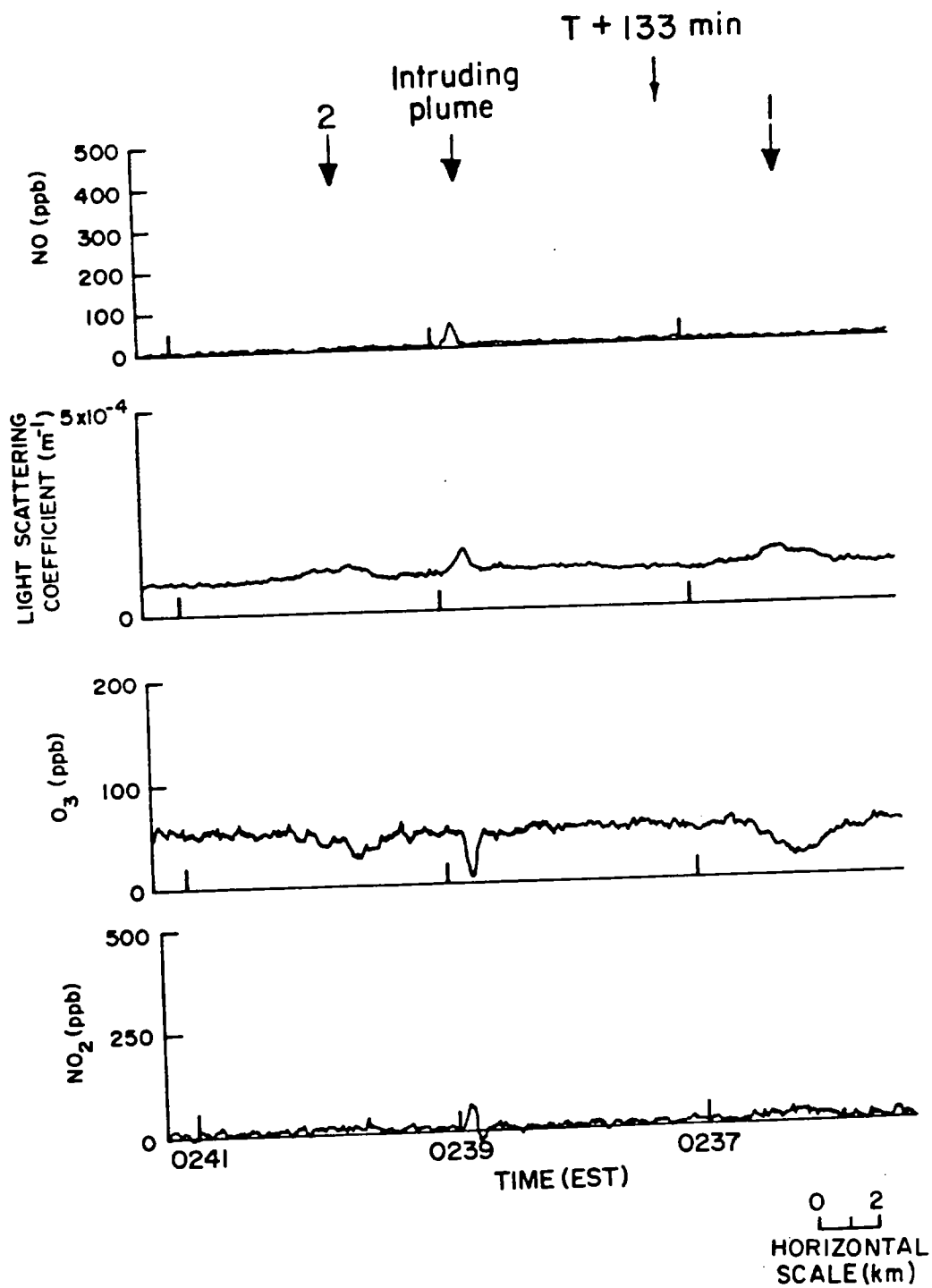


Fig. 9 Measurements in two penetrations (at ~0236 EST and ~0240 EST) of the ground cloud. The signal at ~0239 EST is an intruding plume from a ground source of combustion.

Figure 10 shows the particle size distribution measured at $T + 7$ min in the ground cloud. This number distribution plot shows high concentrations at particle sizes of $\sim 5 \times 10^{-3} \mu\text{m}$ (this is due to combustion and is called the nucleus mode) and a peak in concentrations at particle sizes of $\sim 0.1 \mu\text{m}$ (called the accumulation mode). Since particles of $\sim 0.1 \mu\text{m}$ scatter light very efficiently, the high particle concentrations at this size account for the high light-scattering coefficients in the ground cloud (see Figs. 7 and 8).

The peak in particle concentrations at $0.1 \mu\text{m}$ was slightly suppressed by $T + 25$ min (Fig. 11) as were the concentrations of μm -sized particles. No significant concentrations of particles greater than $10 \mu\text{m}$ in diameter were found after $T + 25$ min. The data in Fig. 11 are replotted in Figs. 12 and 13 in terms of the surface and volume concentrations of particles. It can be seen from these figures that the most of the surface area and volume was contained in particles a few tenths of a micrometer in size.

The characteristics of the ground cloud were still clearly present at $T + 93$ min (Fig. 14) and $T + 126$ min (Fig. 15). However, the ambient air samples (Figs. 16, 17 and 18) also exhibited a significant accumulation mode (as would be expected in a well-aged aerosol), although the nucleus mode is largely absent. While the nucleus mode in the ground cloud may well have been initially due to combustion, and the peak at $0.1 \mu\text{m}$ to the rapid aggregation (i.e. accumulation) of the small particles, the measured particle size distributions suggest that even by $T + 25$ min other particle-generating mechanisms were becoming important within the ground cloud. Figures 10, 11, 14 and 15 show the accumulation mode to be monotonically decreasing with time as the cloud is diluted, while at the same time the nucleus mode continues well above ambient values. This suggests that new nucleus mode particles were still being produced by gas-to-particle conversion in the post-launch period, but that any production of new accumulation mode particles did not keep pace with dilution.

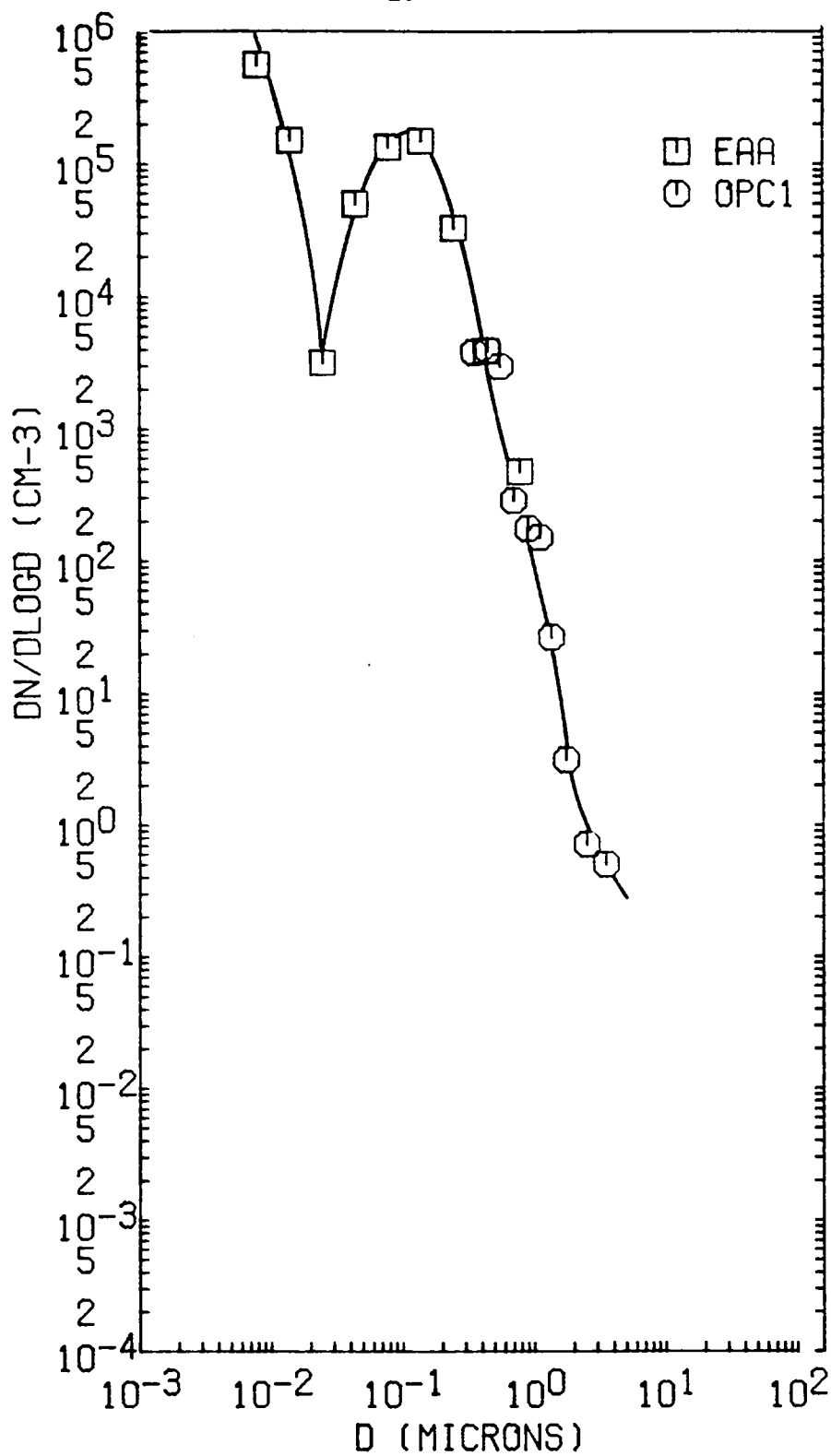


Fig. 10 Point plot of particle number concentration per log size interval $dN/d \log D$ (in units cm^{-3}) versus particle diameter D (in μm) at $T + 7$ min and 610 m AGL in the ground cloud.

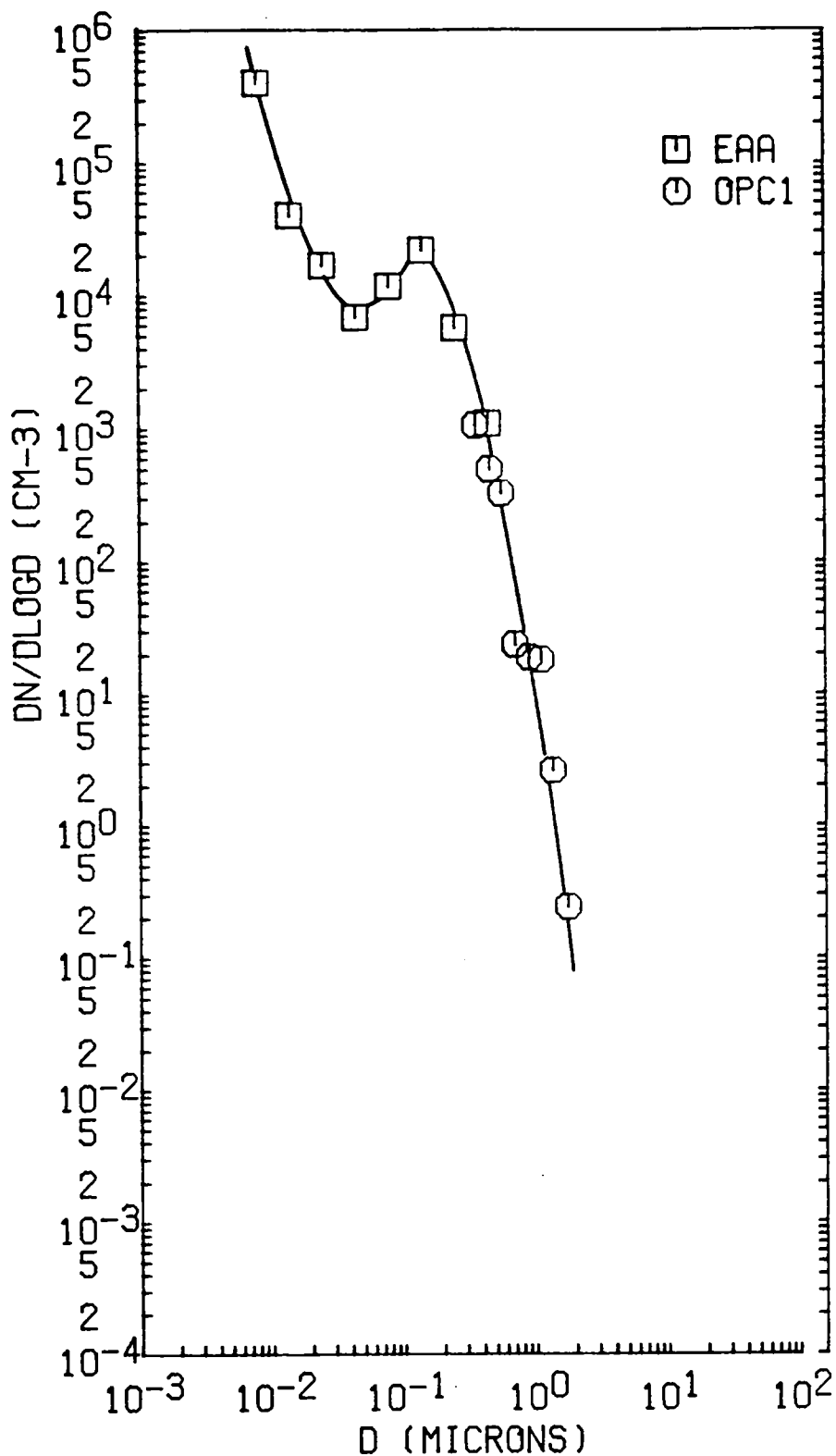


Fig. 11 Point plot of particle number concentration per log size interval $dN/d \log D$ (in units cm^{-3}) versus particle diameter D (in μm) at $T + 25$ min and 549 m AGL in the ground cloud.

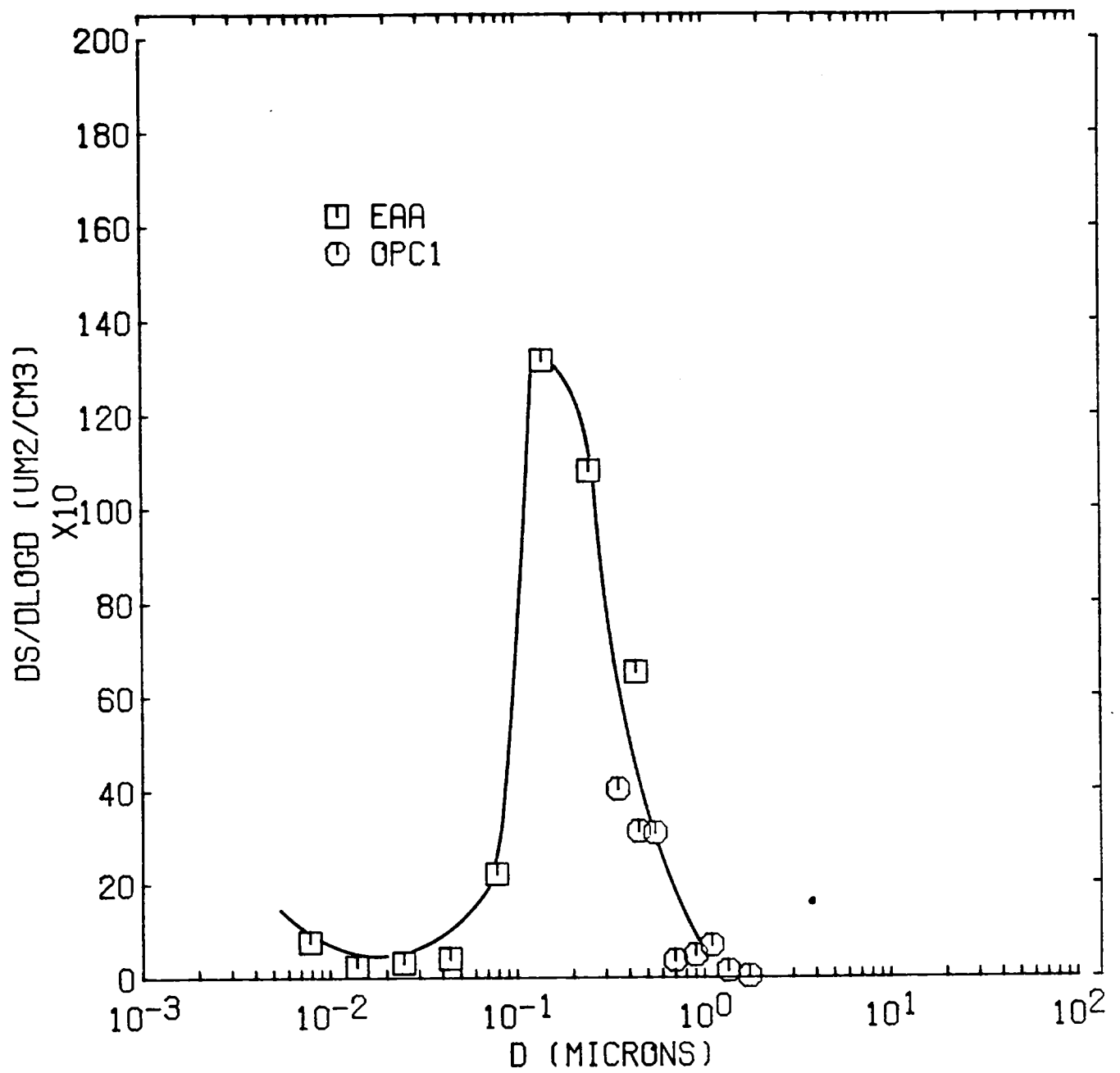


Fig. 12 Point plot of particle surface area concentration per log size interval $dS/d \log D$ (in units $\mu m^2 cm^{-3}$) versus particle diameter D (in μm) at $T + 25$ min and 549 m AGL in the ground cloud.

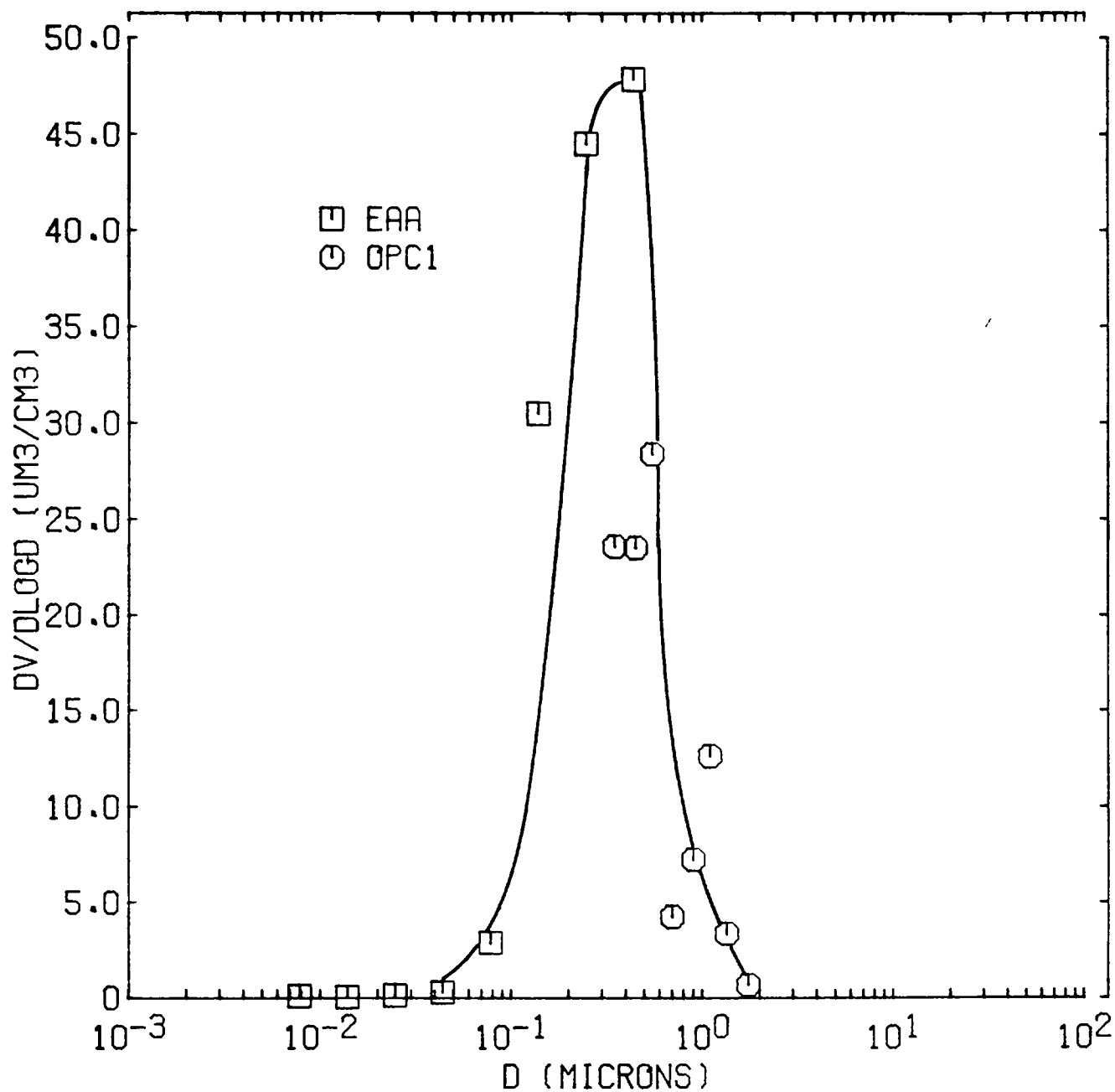


Fig. 13 Point plot of particle volume concentration per log size interval $dV/d \log D$ (in units $\mu\text{m}^3 \text{cm}^{-3}$) versus particle diameter D (in μm) at $T + 25 \text{ min}$ and 549 m AGL in the ground cloud.

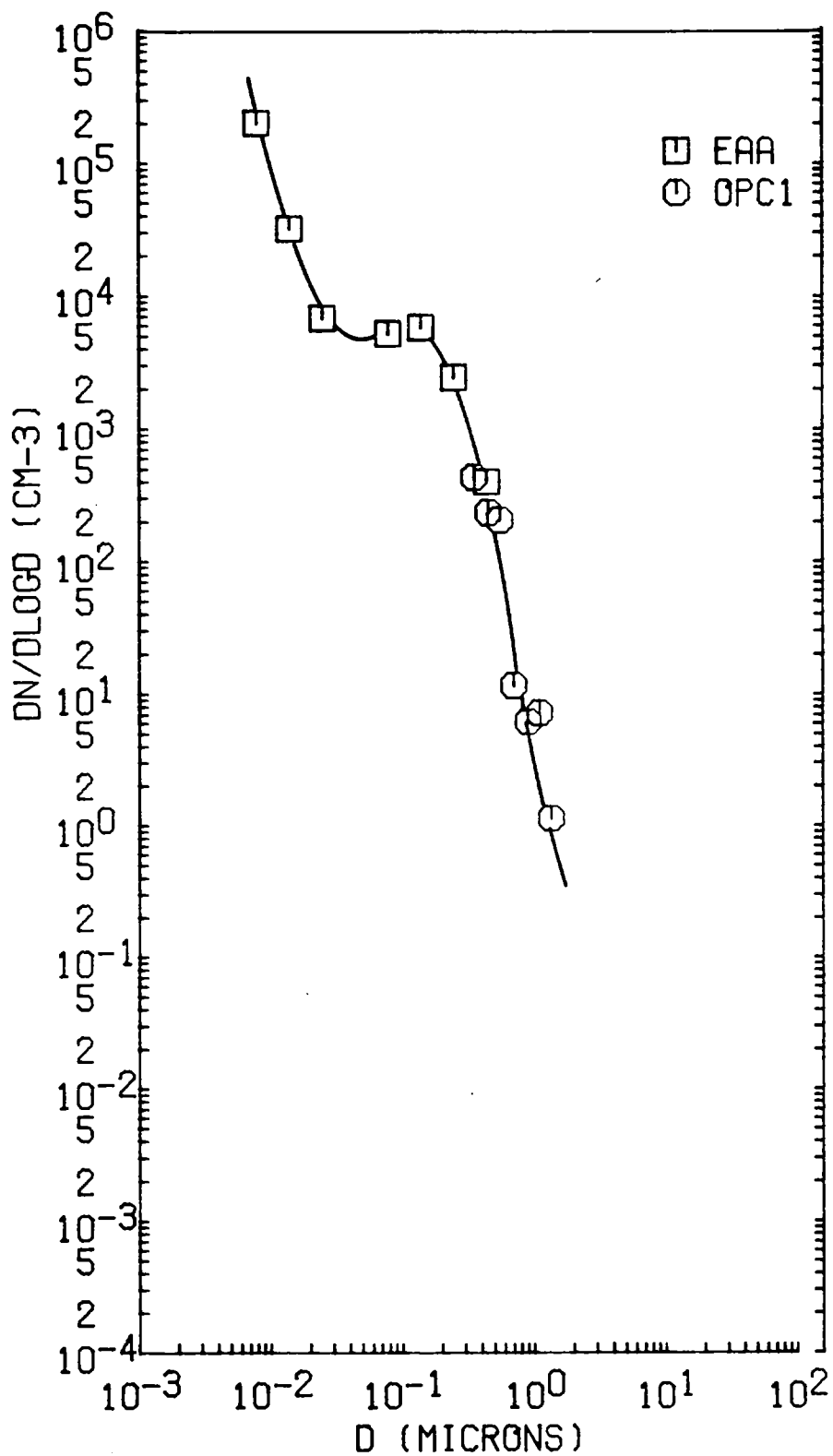


Fig. 14 Point plot of particle number concentration per log size interval $dN/d \log D$ (in units cm^{-3}) versus particle diameter D (in μm) at $T + 93$ min and 518 m AGL in the ground cloud.

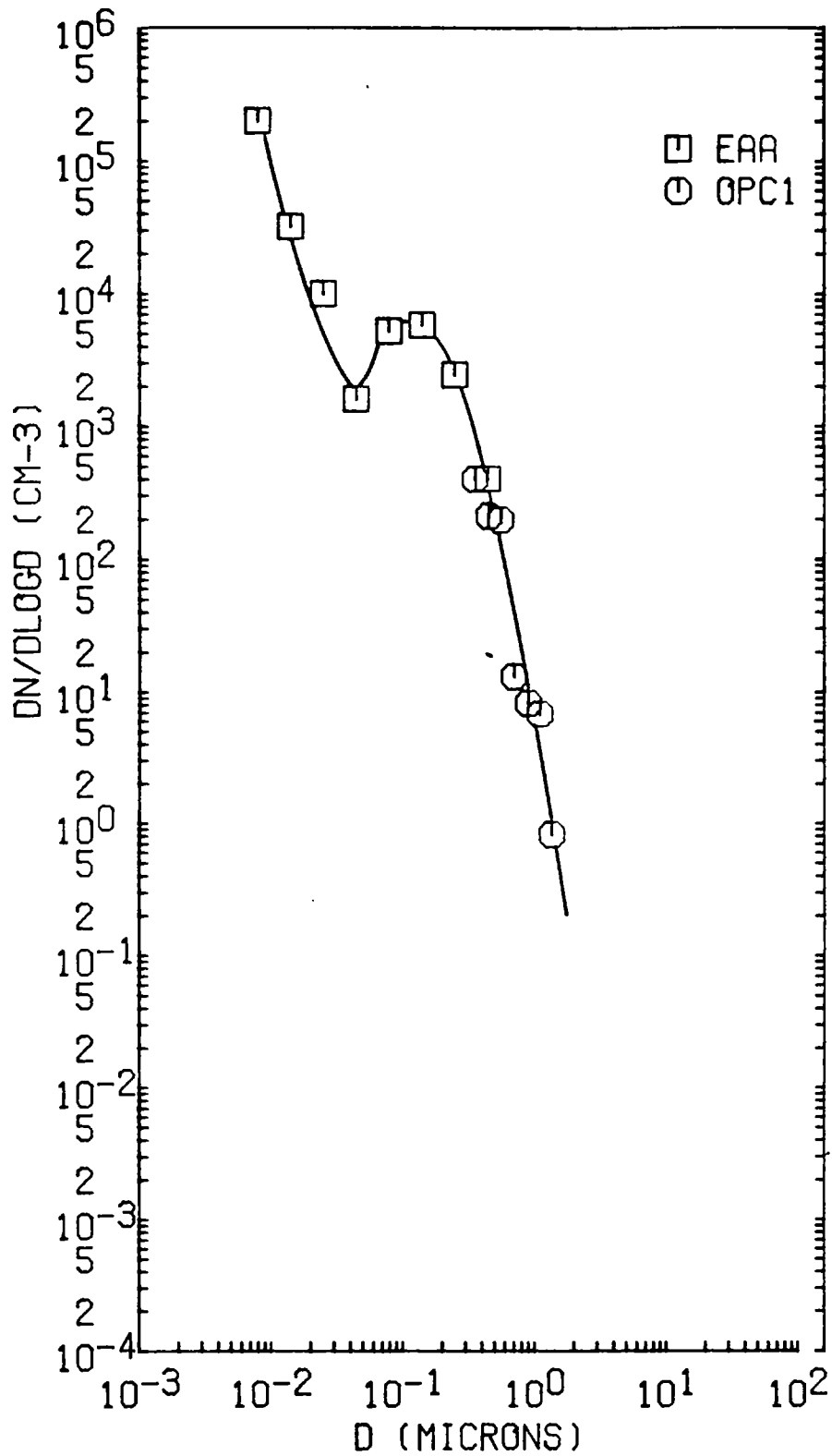


Fig. 15 Point plot of particle number concentration per log size interval $dN/d \log D$ (in units cm^{-3}) versus particle diameter D (in μm) at $T + 126$ min and 518 m AGL in the ground cloud.

It is interesting to note that the ambient particle size distribution was starting to show traces of fog or haze droplets near the end of the sampling period (Figs. 16 and 17). As can be seen in Fig. 18, these few droplets completely dominated the volume concentration. It should be noted that these measurements were obtained with the "ASSP", which is an in situ sampler that measures the sizes of the particles as they exist in the atmosphere (i.e. without pre-drying).

6. Hydrocarbons

Nine measurements of hydrocarbons were made between T + 4 min and T + 174 min using the AID portable gas chromatograph with a 2-meter Chromosorb 102 column. The gas chromatograph was operated so that the methane passed through the column; hydrocarbons were then back-flushed off the rear of the column.

The measured total concentrations of hydrocarbons were identical (within the accuracy of the measurements) in the ground cloud and in the ambient air, both being ~5-6 ppm. The total non-methane hydrocarbon (TNMHC) measurements showed the ground cloud to be relatively rich at 2.5-3.5 ppm (as CH_4) between T + 13 min and T + 28 min, but by T + 47 min it had decreased to background levels (1.0-1.5 ppm). The concentrations of TNMHC which were measured at about 500 m AGL in the ground cloud at night (~4.0 ppm) were comparable to the daytime concentrations measured at the same altitudes in the ambient air on the afternoon (~1600 hrs) after the launch. Since the concentrations of TNMHC in the ambient air during the day are higher than at night, a major daytime source of TNMHC probably exists in the area (e.g. automobiles, photo-organic processes, etc.). Thus, the concentrations of TNMHC even in the thick portions of the ground cloud were within the natural ~24-hr cycle of variations found at this location.

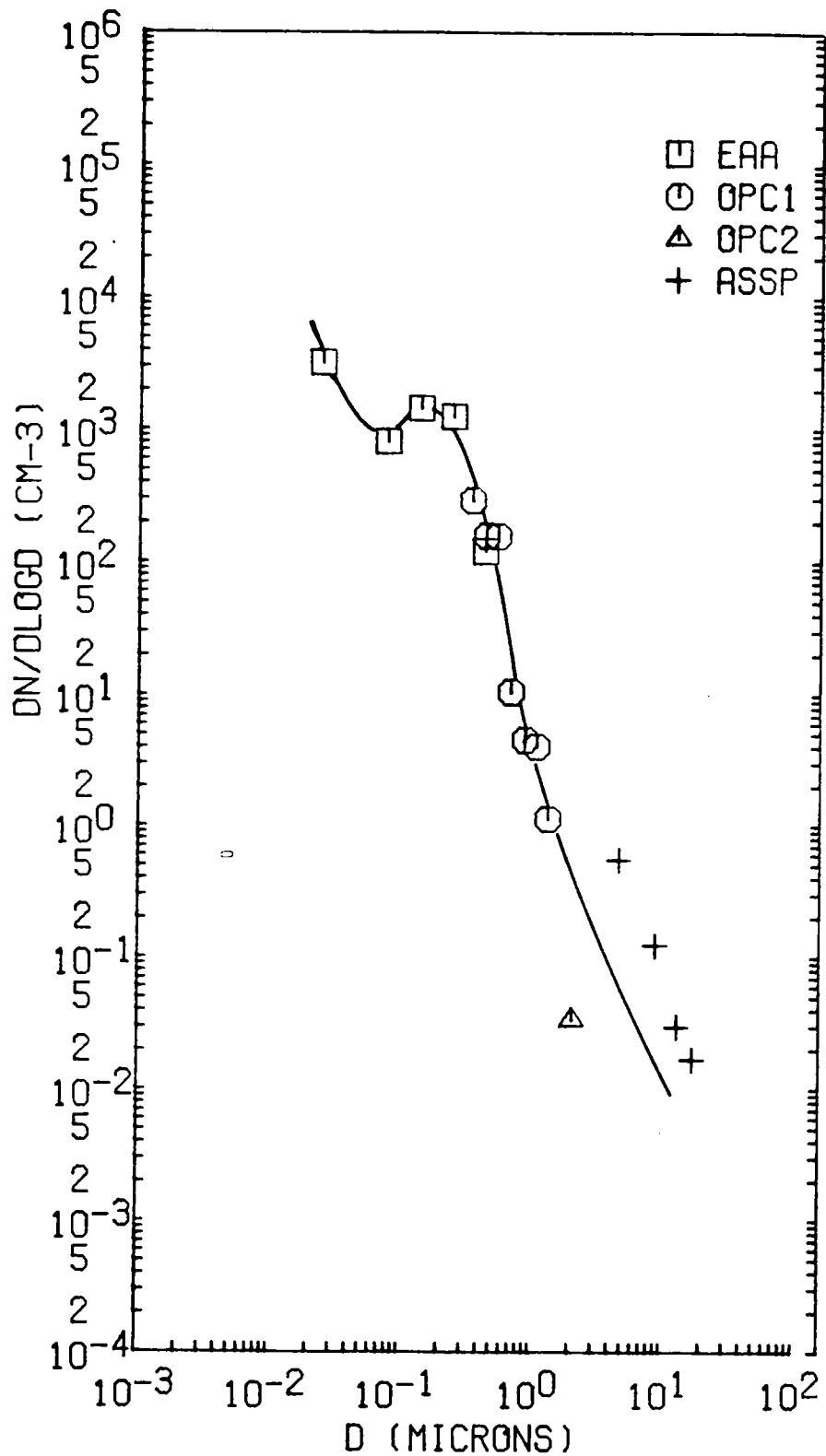


Fig. 16 Point plot of particle number concentration per log size interval $dN/d \log D$ (in units cm^{-3}) versus particle diameter D (in μm) in the ambient air at 549 m AGL.

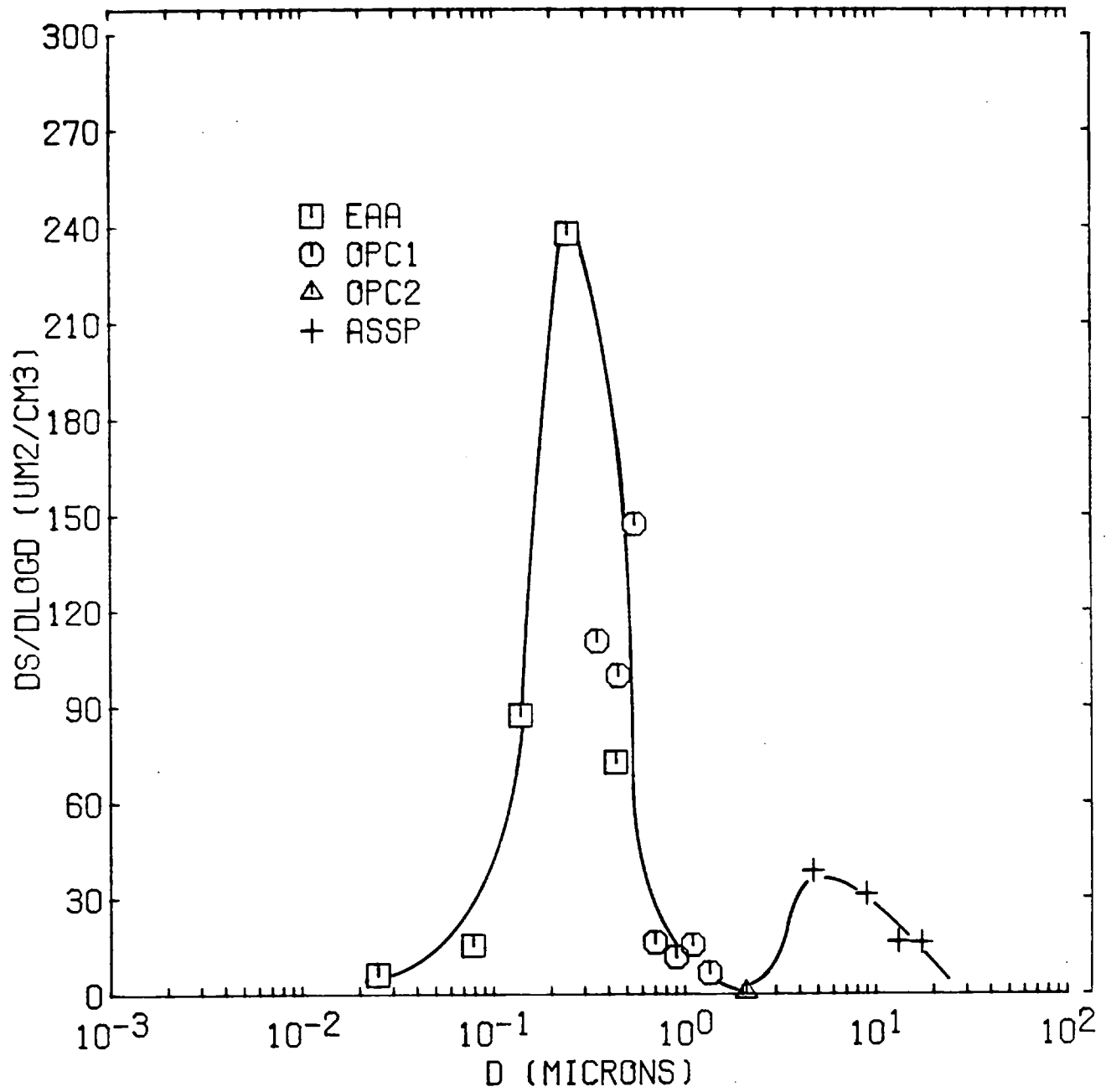


Fig. 17 Point plot of particle surface area concentration per log size interval $dS/d \log D$ (in units $\mu m^2 cm^{-3}$) versus particle diameter D (in μm) in the ambient air at 549 m AGL.

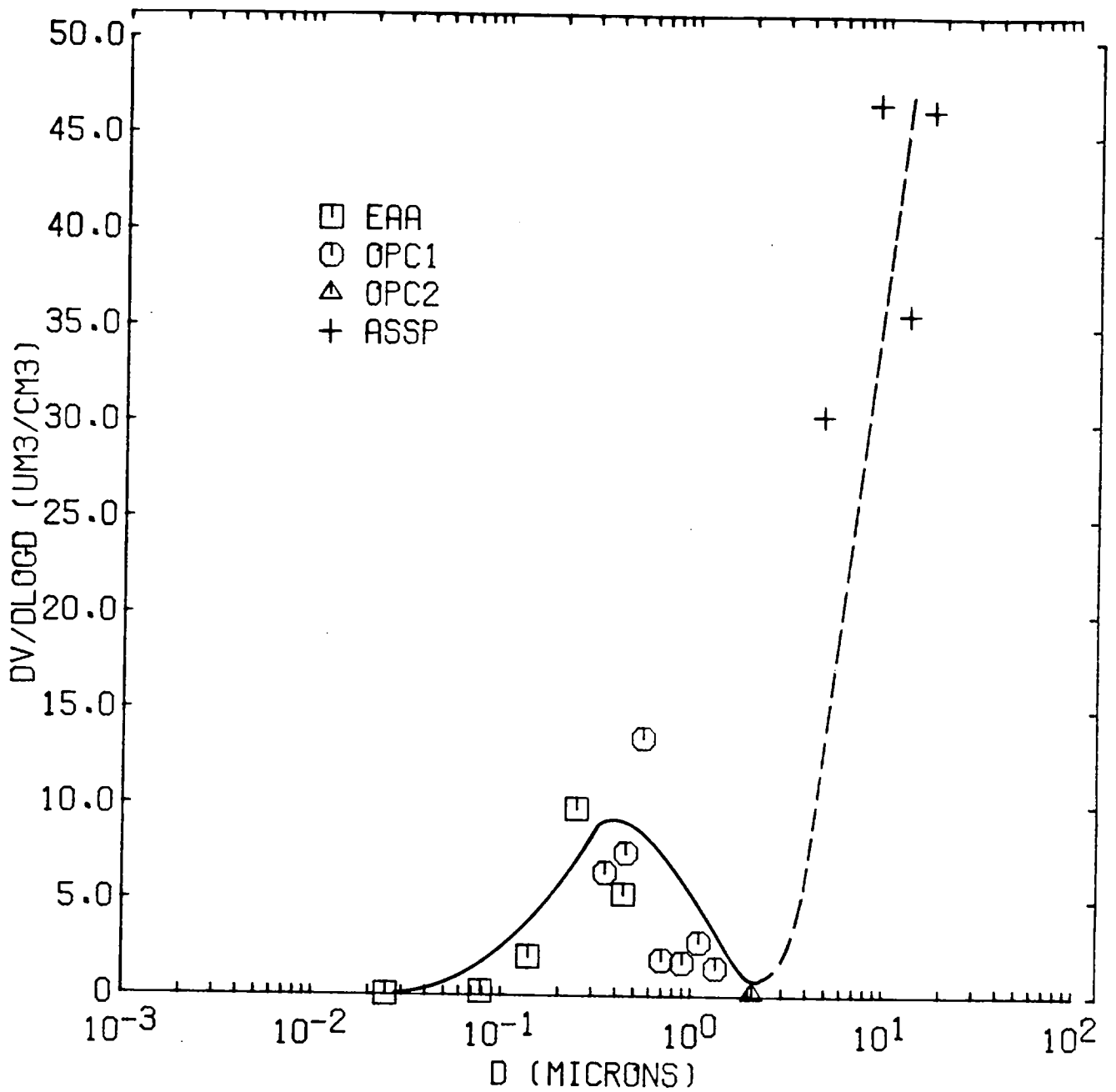


Fig. 18 Point plot of particle volume concentration per log size interval $dV/d \log D$ (in units $\mu\text{m}^3 \text{cm}^{-3}$) versus particle diameter D (in μm) in the ambient air at 549 m AGL.

7. Volumes and emission factor of the ground cloud

After the ground cloud had stabilized at the marine inversion, its dispersion was essentially limited to the horizontal plane. The horizontal extent of the plume could be deduced since most of the aircraft penetrations were made in orthogonal pairs (see Appendix B). It was assumed that the ground cloud was rectangular in shape, 100 m thick, and that one pass in each pair was along the length of the rectangle and the other pass along the width of the rectangle. In this way, estimates of the volume of the ground cloud as a function of time could be obtained (Fig. 19).

It can be seen from Fig. 19 that the relationship between the volume V of the ground cloud and the time t after launch is of the form:

$$V = V_0 t^\alpha \quad (1)$$

where, V_0 is the initial volume and α is a constant.

If t is in minutes, the best-fit line to the data in Fig. 19 gives:

$$V_0 = 1.31 \times 10^6 \text{ m}^3 \text{ and } \alpha = 0.98$$

Those results are in reasonable agreement with the empirical K-theory of dispersion (Smith, 1957) which gives a dispersion rate proportional to $t^{1/2}$ for each dimension. Thus, with vertical dispersion constrained, a volume growth proportional to t (i.e. $\alpha = 1$) would be predicted by K-theory, compared to our value of $\alpha = 0.98$.

The dispersion rate of the ground cloud may also be estimated from the measurements of the mass concentration of particles ($<2 \mu\text{m}$ in diameter)* that were measured near the center of the ground cloud.

* The measured particle size distribution showed that after the initial gravitational settling of the very large particles from the pad debris, most of the particles in the ground cloud were $<2 \mu\text{m}$ in diameter (see §5).

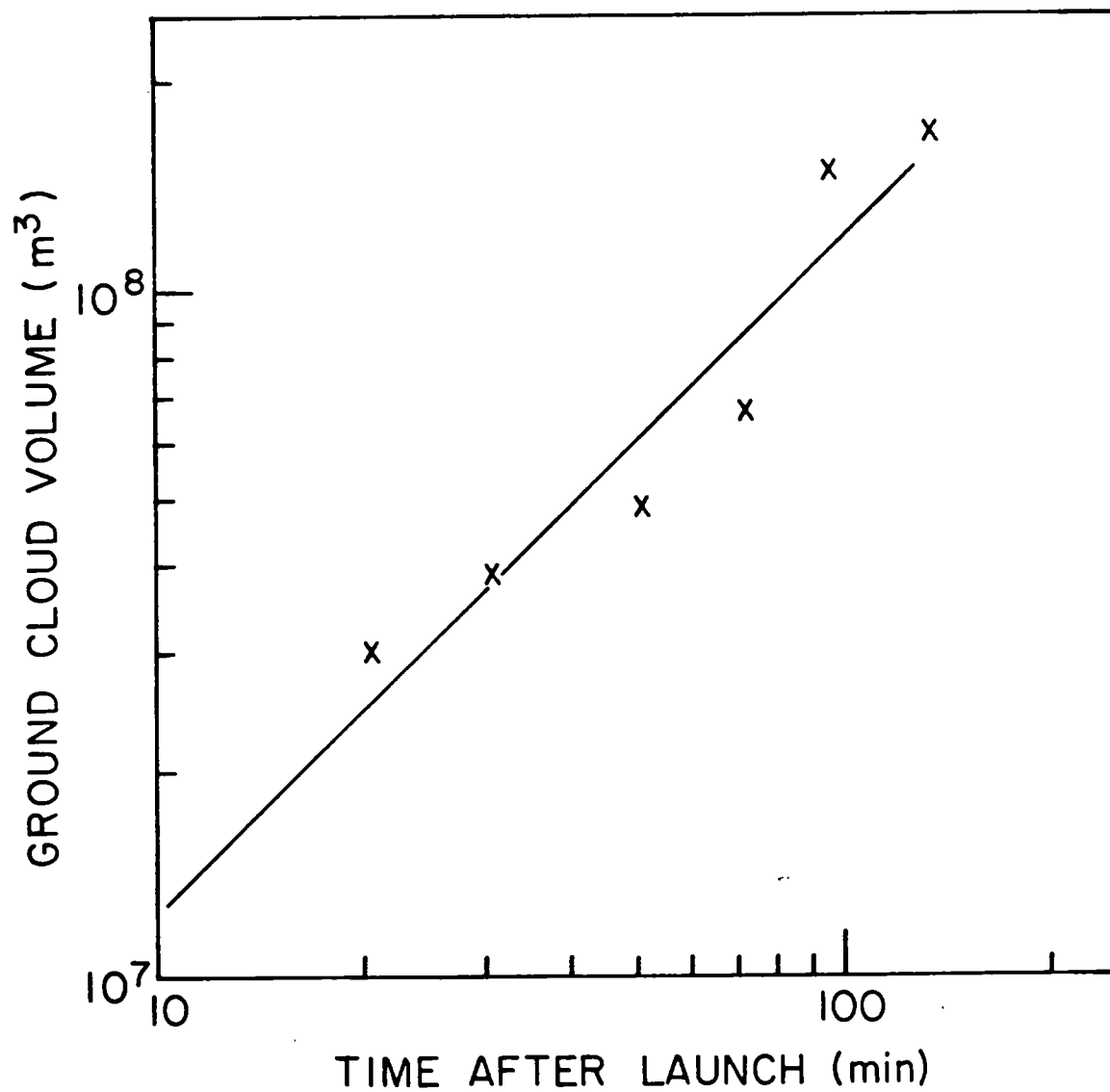


Fig. 19 Estimates of the volume of the ground cloud as a function of time.

These data are shown in Fig. 20, where it can be seen that the mass concentrations M at time t is given by:

$$M = M_o t^b \quad (2)$$

where, if t is in minutes:

$$M_o = 1.44 \times 10^3 \mu\text{g m}^{-3} \text{ and } b = -0.91$$

This relation provides good support for the previously described volume measurements and supports our assumption that dispersion of the ground cloud in the vertical was negligible.

Also plotted in Fig. 20 is the concentration of NO in the ground cloud as a function of time. The concentration (C) of NO at time t is given by:

$$C = C_o t^d \quad (3)$$

where,

$$C_o = 5.686 \times 10^3 \text{ ppb and } d = -1.22$$

The difference between eqns. (1), (2) and (3) is probably due to the fact that NO disperses and reacts to form NO_2 (see §9).

The above measurements can be used to estimate the fraction of the emitted propellant material that remained in the stabilized ground cloud. Using the volume estimates made at approximately 0045, 0055, 0115 and 0135 EST, and multiplying these by half the measured peak mass concentration of particles (1/2 in order to reduce the peak mass concentration to an approximate cloud average concentration), we obtain an estimate for the total mass of particles in the ground cloud of $1.16 \pm 0.25 \text{ kg}$. Now, 9800 kg of propellant were burned during the hold-down period and the rise of the rocket to 1000 m. Hence, the percentage of the propellant material that remained in the ground cloud (i.e. the emission factor) was $(0.012 \pm 0.002)\%$.

* The measured particle size distribution showed that after the initial gravitational settling of the very large particles from the pad debris, most of the particles in the ground cloud were $<2 \mu\text{m}$ in diameter (see §5).

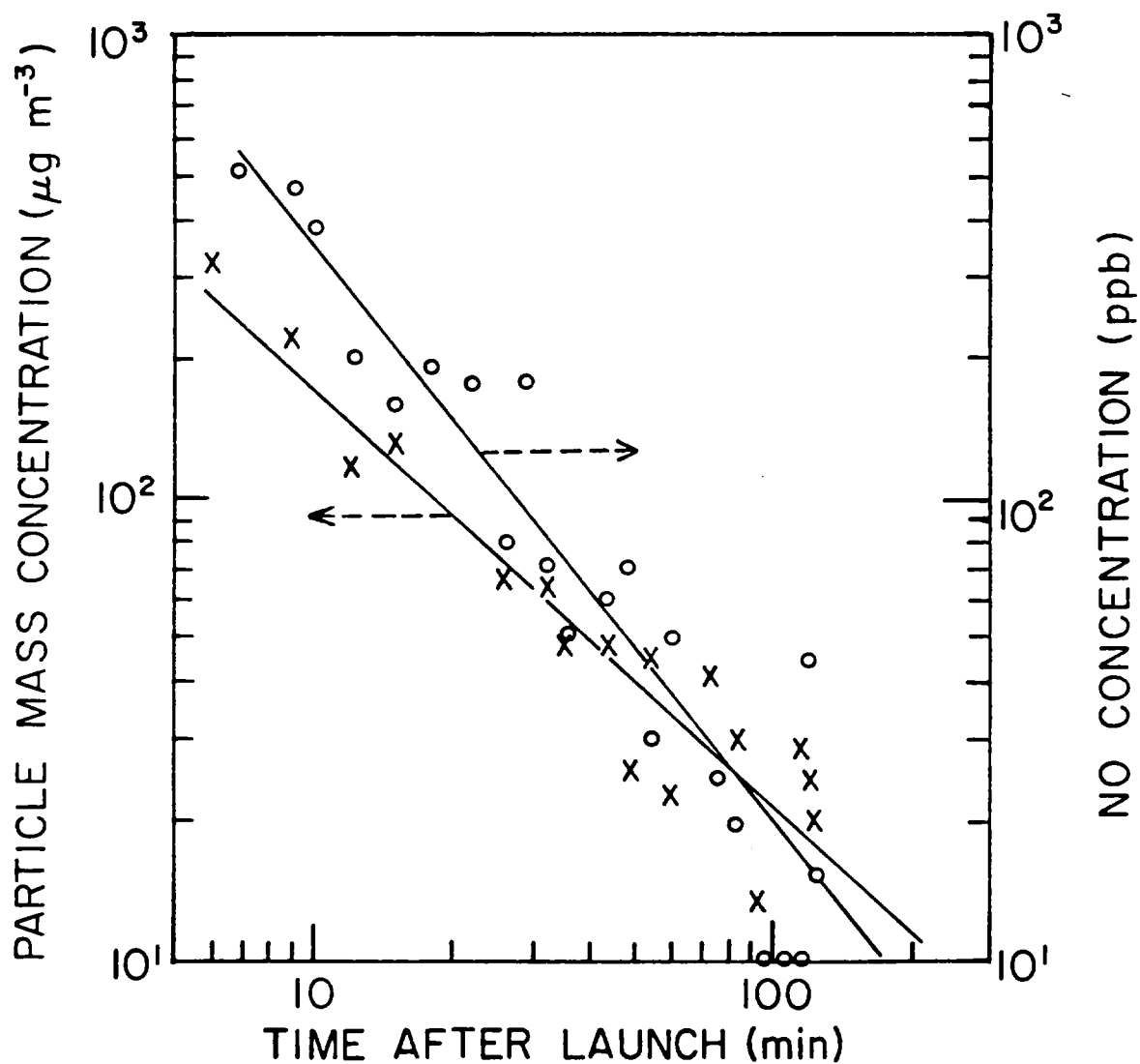


Fig. 20 The crosses show the total mass concentration of particles ($<2 \mu\text{m}$ in diameter) in the ground cloud. The circles show the peak concentrations of nitric oxide in the ground cloud.

This relatively low value of the emission factor indicates an efficient combustion process, more efficient, for example, than modern coal-fired power plants (which have emission factors of ~0.05%) or fires associated with the burning of wood waste (which have emission factors of ~1%).

8. Average density of the particles in the ground cloud

Shown in Fig. 21 are measurements of the mass concentration of particles plotted against their volume concentrations between T + 6 min and T + 60 min. The slope of the best-fit line to the datum points in Fig. 20 gives the average density of the particles in the ground cloud. Apart from the measurement at T + 6 min, the particle density is seen to remain reasonably constant at 1.1 g cm^{-3} . The measurement at T + 6 min was taken just after the larger particles were observed to be falling out of the ground cloud (see Fig. 4). The density of these large particles was 2.08 g cm^{-3} . This higher density is consistent with the observations of pad debris (concrete?) found in the impaction samples during the initial penetrations.

9. Trace gas reactions

The concentrations of SO_2 in the ground cloud were quite low, decreasing to background levels by T + 20 min (see §4).

The behavior of O_3 and NO_x was interesting and reveal some further characteristics of the ground cloud.

Since our measurements were obtained at night, we can assume that the only reaction* of importance in the NO_x — O_3 cycle was:



* Some O_3 may also have been eliminated by particle oxidation, however, the conversion to NO_2 is rapid enough to account for all of the O_3 that was removed.

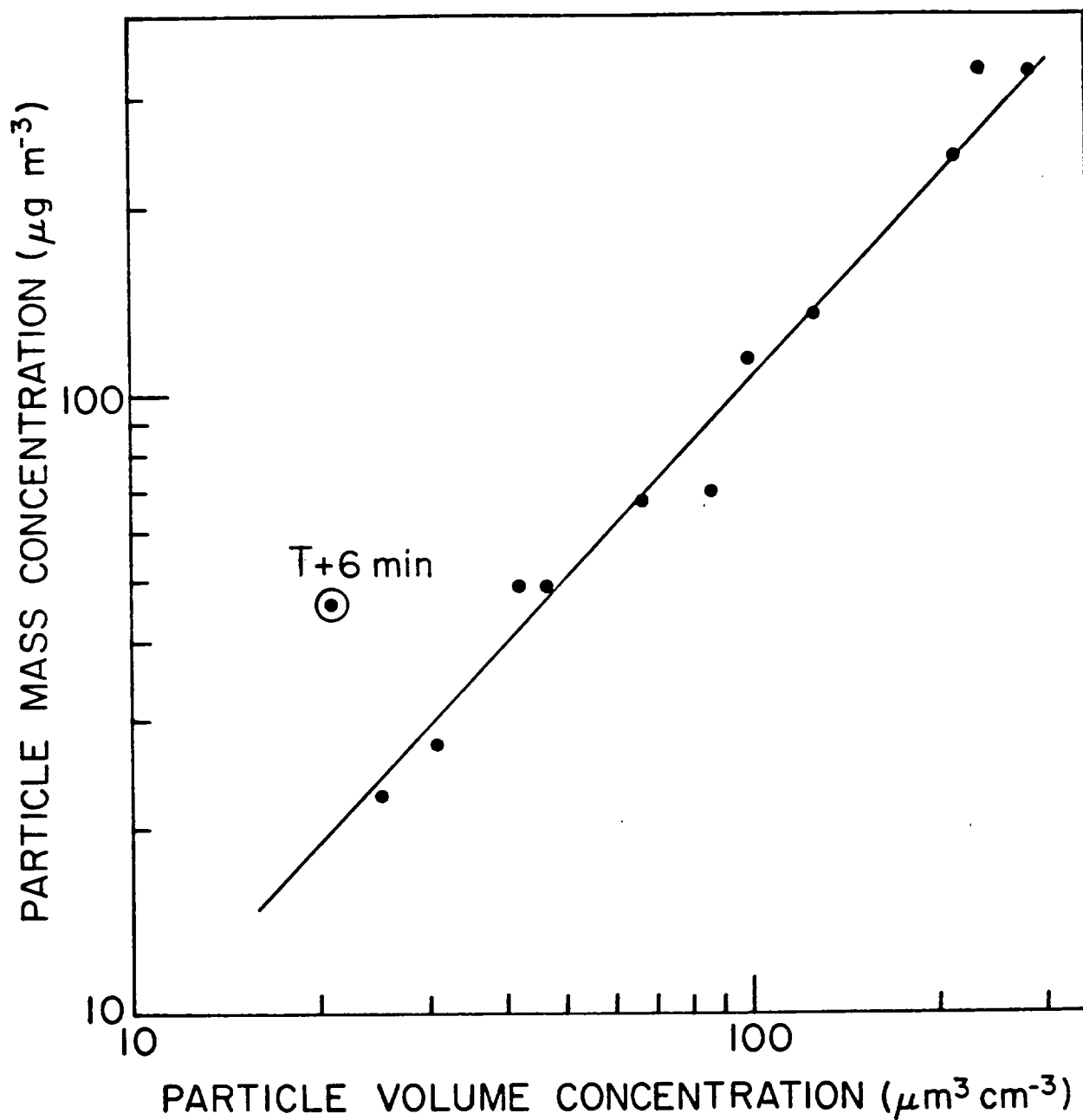


Fig. 21 Mass concentration of particles versus their total volume concentration ($<2 \mu\text{m}$ in diameter) in the ground cloud from $T + 6 \text{ min}$ to $T + 60 \text{ min}$.

In this case the NO_2/NO ratio should increase monotonically with time.

In fact, this ratio increased during the first hour and then became approximately constant (see data in Appendix C). Since the O_3 levels were strongly depressed in the ground cloud, this suggests that the conversion of NO to NO_2 was limited by the rate at which ambient ozone could diffuse into the ground cloud. Initially, ambient ozone was probably mixed efficiently into the ground cloud by mechanical turbulence but, as the turbulence died away, the O_3 diffused more slowly into the cloud.

We may check the above ideas by comparing the rate of loss of NO [calculated from the rate constant for eqn. (4)] with the conversion rate based on measured ratios of NO and O_3 . The rate constant for eqn. (4) at 17°C is $1.4 \times 10^{-14} \text{ cm}^3 \text{ molecule}^{-1} \text{ s}^{-1}$ (Anderson, 1976). Hence the rate of loss of NO would be:

$$\frac{1}{\text{NO}} \frac{d(\text{NO})}{dt} \approx 70 \text{ hr}^{-1} \text{ (for an ambient } \text{O}_3 \text{ concentration of 50 ppb).}$$

The measured initial loss rate of NO (assuming that the concentration of NO_2 in the ground cloud was initially zero) was 5.5 hr^{-1} . However, between $T + 9 \text{ min}$ and $T + 90 \text{ min}$, the measured average loss rate of NO was only 0.25 hr^{-1} . This clearly suggests a process limited by mixing.

10. Production of cloud condensation nuclei

Cloud condensation nuclei (CCN) are those particles in the air which serve as nuclei upon which cloud and fog droplets form. Although CCN are often only a small fraction of the total atmospheric aerosol, they play an important role in determining the colloidal stability of clouds and the formation of precipitation.

It can be seen from the measurements plotted in Fig. 22 that the ground cloud was rich in CCN, the concentrations in the cloud being about a factor of four larger than those in the very dirty ambient air^{*}. It is interesting to note that the concentration of CCN at 0.5% supersaturation in the ground cloud is roughly constant between T + 24 min (0048 EST) and T + 110 min, while the CCN at 0.2% supersaturation declined monotonically with time (roughly by a factor of 2) during the same time period. From the measurements of the volume of the ground cloud (§7) and the CCN concentrations at T + 24 min, the initial ~~rate of~~ production of CCN at 0.5% supersaturation in the ground cloud is computed to be $\sim 1.2 \times 10^{17}$ CCN ~~s~~⁻¹. This rate should be compared with the global anthropogenic CCN emissions of 2×10^{21} CCN s⁻¹ (Radke and Hobbs, 1976) or $\sim 10^{16}$ CCN s⁻¹ from the city of Denver (Squires, 1966).

Our measurements also suggest that additional CCN formed within the ground cloud as it moved through the atmosphere. Since the volume of the ground cloud increased by $\sim 10^8$ m³ between T + 24 and T + 110 min while the concentration of CCN remained roughly constant, this gives an in-cloud production rate of ~ 1 CCN cm⁻³ s⁻¹. It is not known whether these CCN are new particles or smaller particles that have grown by coagulation or gas-to-particle condensation.

11. Meteorological influences on ambient air samples in the vicinity of Cape Canaveral

Clear skies and warm air were typical surface conditions throughout Florida on November 12th and 13th, as the region remained under the influence of a high-pressure system centered to the north. Winds were light and generally from

* Unpolluted maritime and continental airmasses often have CCN concentrations lower by a factor of ~ 50 than those in the ambient air at Cape Canaveral at the time of our measurements.

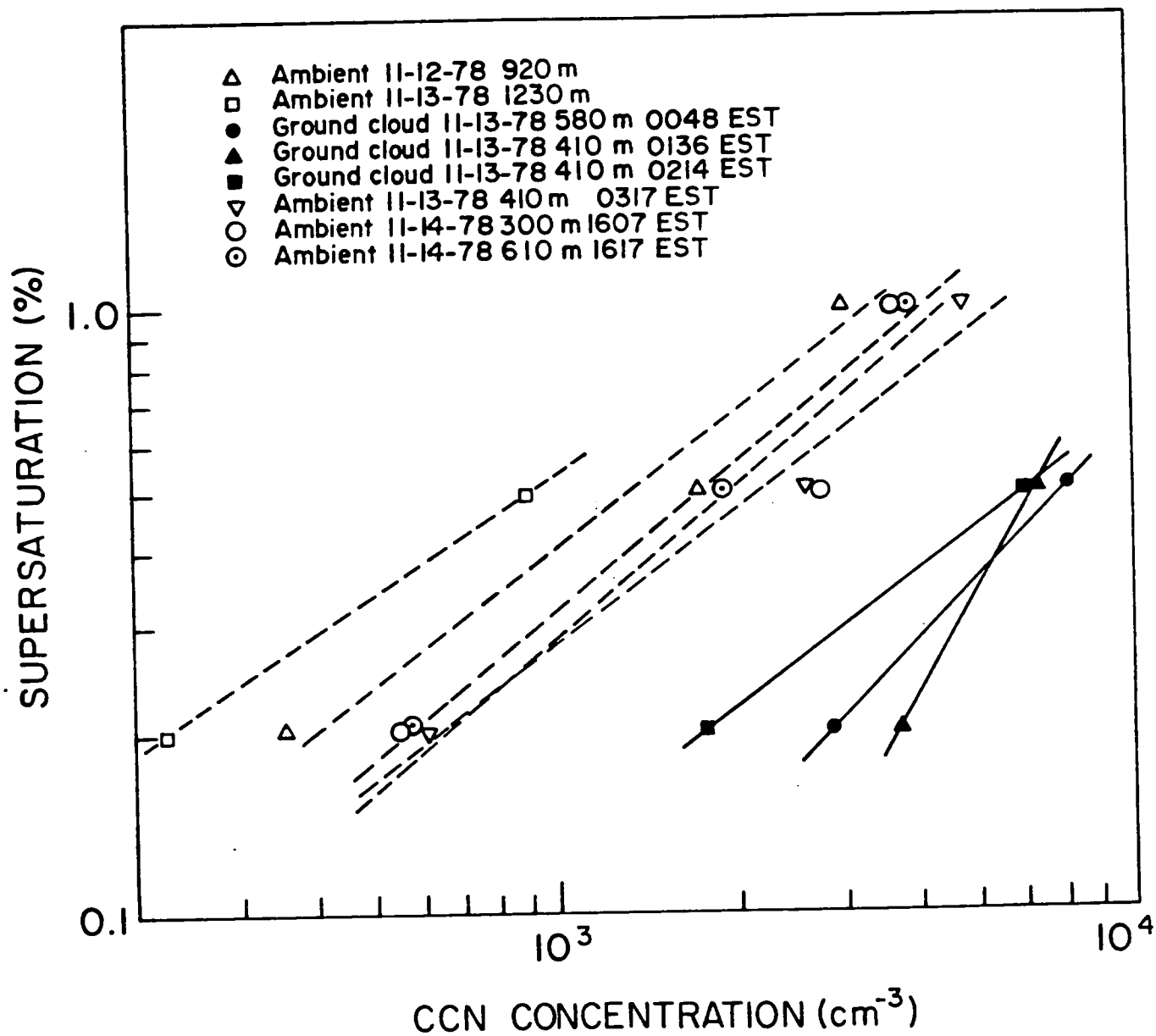


Fig. 22 Concentrations of cloud condensation nuclei (CCN) as a function of supersaturation in the ground cloud and in the ambient air at the time of the launch.

the north, which helped create foggy mornings and hazy afternoons. A weak cold front passed through Florida late in the day on the 13th, causing isolated showers and cloudy skies along the eastern coast. Conditions improved on the 14th as an upper-level ridge moved over the area.

As a result of these synoptic changes, the pre- and post-launch measurements in the ambient air on the afternoons of November 12 and 13, as well as the measurements obtained in the clouds of materials from the rocket, were all in somewhat different airmasses. The pre-launch airmass was southern continental, while the airmass at the time of the launch was more northern continental with a substantial overwater modification. The length of the overwater modifications decreased during the day on the 13th.

Despite the obvious differences in airmass during the pre- and post-launch measurements, all of the measurements in the ambient air at 600-1000 m were remarkably similar. In each case there was a moderate haze (light-scattering coefficient $\sim 5 \times 10^{-5} \text{ m}^{-1}$), a fine particle mass loading of $5\text{-}20 \text{ } \mu\text{m m}^{-3}$, and SO_2 concentrations of 7-10 ppb. Ozone showed a slight decreasing trend from 60 to 40 ppb between the 12th and 13th November. Methane concentrations were about 6 ppm while total non-methane hydrocarbons were about 4 ppm (as methane) on the afternoon of the 13th.

The particle size distributions maintained the well-aged appearance shown in Fig. 16, with only two significant departures. Firstly, in Fig. 16 the nucleus mode below $10^{-2} \text{ } \mu\text{m}$ is absent, but it was present on the afternoon of the 13th in concentrations $\sim 10^5 \text{ cm}^{-3}$. Evidently sunlight photolyzed gas-to-particle conversion was taking place in the rich "soup" of trace gases that covers large portions of the eastern United States with a rather uniform blanket of pollution. Secondly, while the particle size distributions on

November 12 displayed the prominent 0.1-0.2 μm peak seen in Fig. 16, this feature was absent in the post-launch ambient air.

We also obtained some particle size distribution measurements in the vicinity of Cape Canaveral on March 16, 1978 when the meteorological conditions were similar to those on November 12-14, 1978. The earlier measurements showed particle size distributions for particles $>0.1 \mu\text{m}$ nearly identical to those obtained in November. However, the nucleus mode was even stronger (peak concentrations 10^6 cm^{-3}) than that observed on the afternoons of November 12 and 13.

We conclude that the ambient particle distributions at Cape Canaveral, for particles $>0.1 \mu\text{m}$, are similar to those of any well-aged eastern continental airmass. The presence of the nucleus mode may be due to local sources of pollution, but it is more likely due to fresh particles being produced by a photolyzed gas-to-particle conversion reaction.

12. Summary and Conclusions

A series of airborne measurements have been obtained of the particles and trace gases in the clouds of effluent produced by a night-time launch of an Atlas/Centaur rocket. The principal findings of this study are:

- Due to very dry conditions above the marine layer, the launch pad cloud and portions of the flame trench cloud were subsaturated and contained no detectable liquid water within 3 min of launch.
- The launch pad and flame trench clouds contained a high mass concentration ($\sim 1 \text{ g m}^{-3}$) of millimeter-sized pieces of launch pad debris but these were rapidly removed by sedimentation.

- The launch pad cloud rapidly subsided to the top of the marine layer where it combined with the flame trench cloud to produce the ground cloud.
- Due to the stable atmospheric conditions, the ground cloud remained elevated and diffused slowly and almost entirely in the horizontal plane. The ground cloud was easily identified by relatively high concentrations of NO and NO₂ and by very low (~0) concentrations of O₃. The rates of conversion of NO to NO₂ (by reacting with the ambient O₃) also reflected the slow rate of mixing of the ground cloud with the ambient air. The ground cloud remained an identifiable entity for at least 135 min after launch. At this time it mixed with an industrial plume and the airborne measurements were terminated.
- The concentrations of hydrocarbons in the ground cloud were low. The methane concentrations in the ground cloud were not significantly different from the ambient concentrations. The total non-methane hydrocarbons in the ground cloud were initially slightly higher than in the ambient air, but within 47 min of the launch they had declined to the ambient concentrations.
- The particles in the ground cloud contained two prominent particle modes, one centered around 5×10^{-3} μm diameter and the other around 0.1 μm diameter. There is some evidence to suggest that the former mode was produced by gas-to-particle conversion and the latter mode by directly injected material.

- 25 min after the launch most of the mass of particles in the ground cloud were contained in particles less than a few micrometers in diameter. The particle mass remained fairly constant for at least 70 min after the launch.
- The average density of the particles in the ground cloud was $\sim 1.1 \text{ g cm}^{-3}$.
- The total mass of particles in the ground cloud was surprisingly small ($\sim 1 \text{ kg}$) considering the amount of propellant that was burned. The emission factor was estimated to be 0.012%.
- The concentrations of cloud condensation nucleus (CCN) in the plume were meteorologically significant. The initial emission was $\sim 1.2 \times 10^{17}$ CCN (active at 0.5% supersaturation). In addition, CCN active at 0.5% supersaturation were produced in the ground cloud at a rate of $\sim 1 \text{ CCN cm}^{-3} \text{ s}^{-1}$. CCN active at 0.2% supersaturation did not appear to be produced in the ground cloud.

The above conclusions must be tempered by the recognition that they are based on measurements obtained in only one launch and that the launch conditions may significantly affect the nature of the ground cloud. For example, the ground cloud that we studied was saturated only very briefly. A similar launch with a long-lived supersaturated cloud might be expected to have a significantly smaller nucleus mode (due to particle-droplet coagulation) and to contain lower concentrations of particles $> 0.1 \text{ } \mu\text{m}$ (including CCN) due to droplet-droplet coagulation and possible precipitation removal. Some trace gases, especially SO_2 , might also be efficiently removed in the presence of droplets. Secondly, our measurements were obtained in a night-time launch; this eliminated gas-to-particle conversion processes that are catalyzed by sunlight. Finally, the

very stable atmospheric conditions under which the ground cloud was transported permitted high concentrations of particles to exist in the ground cloud for an extended period of time and inhibited their transport to the ground. The low rates of mixing of the ground cloud with the ambient air also resulted in slow, diffusion-limited conversion of NO to NO₂ in the ground cloud.

ACKNOWLEDGMENTS

Special thanks are due to the pilot of our research aircraft (Mr. S. Nickells) whose skilled airmanship contributed greatly to the success of this project. Thanks are also due to other members of the aircrew (M. Learned and R. Fabro) and members of our Cloud and Aerosol Research Group who contributed to this study (especially to T. Walker for the aircraft position plots and J. Werth for the trajectory analyses).

REFERENCES

- Anderson, L. G., 1976: Atmospheric chemical kinetics data survey. Rev. Geophys. Space Phys., 14, 151.
- Danielsen, E. F., 1961: Trajectories: isobaric, isentropic and actual, J. Meteor., 18, 479.
- Hindman, E. E., II, and Grant, L. O., 1979: Elemental compositions of aerosol particles and ice nucleus concentrations in the ground cloud from the Atlas/Centaur launch, 13 Nov 1978. Report to Argonne National Laboratory (in preparation).
- Radke, L. F. and P. V. Hobbs, 1976: Cloud condensation nuclei on the Atlantic seaboard of the United States. Science, 193, 999.

Smith, F. B., 1957: The diffusion of smoke from a continuous elevated point-source into a turbulent atmosphere. J. Fluid Mech., 2, 49.

Squires, P., 1966: An estimate of the anthropogenic production of cloud nuclei, J. Rech. Atmos., 2, 297.

APPENDIX A

THE UNIVERSITY OF WASHINGTON'S AIRBORNE ATMOSPHERIC RESEARCH FACILITY

A.1 The Aircraft

The University of Washington's airborne atmospheric research facility, which was used in this study, is mounted aboard a Douglas B-23 aircraft. This is a heavy (12,000 kg) twin-engine aircraft that has proven nearly ideal for atmospheric research in the troposphere. It provides a stable sampling platform at speeds between 35 and 85 m s⁻¹ (60 m s⁻¹ normal sampling speed) and has a service ceiling in excess of 8,000 m. Its low cruising speed greatly eases problems associated with sampling small particles. The B-23 can carry more than 1000 kg of instruments and a crew of seven. Its oversize control surfaces and rugged construction permit excellent maneuverability at all flight levels. The aircraft is equipped for all-weather flying; all leading edges and propellers are deiced and the aircraft is fully equipped for instrument flight rule operations.

A.2 Data System and Basic Parameters

One of the most important characteristics of the facility is that, despite its extent and complexity, an adequate crew can be carried aboard to ensure its reliable operation. Moreover, the crew is provided with sufficient real-time data so that project goals can be adjusted in-flight to take advantage of unique opportunity situations.

Data synthesis is orchestrated by the Flight Data Engineer interacting with a minicomputer (16-bit word, 16K-word capacity coupled to twin 100K-word floppy disks). The Engineer can provide the research crew with any recorded

or computed parameter via more than 20 digital and electromechanical displays, a hard-copy digital printer, and a six-channel, high speed, strip chart recorder.

Data are recorded on both magnetic tape and disk media via serial digital, IRIG FM and direct recording. The disk record allows a detailed flight summary to be compiled immediately after landing at the airport using a small mobile computer.

For this study the aircraft was configured for cloud, particle and trace gas measurements. The instrumentation layout is shown in Fig. A.1. Instruments for measuring basic parameters (temperature, dew point, pressure altitude, altitude above terrain, true airspeed, vertical and horizontal winds, aircraft altitude and rate of climb, turbulence and solar irradiance) are located primarily in the forward portion of the aircraft and are a permanent installation. A history of the aircraft flight path is provided by an x-y plotter which is driven by the aircraft navigational system; this provides a tracing of the aircraft position on a sectional map.

A.3 Particle and Trace Gas Instrumentation

A schematic of the layout and ducting for the particle and trace gas instrumentation is shown in Fig. A.2. The most complex portion is the particle sizing system which consists of four instruments which are completely integrated and controlled by the onboard computer. These provide size spectral measurements of atmospheric particles from 0.01 to 65 μm in diameter over a concentration range of 10^{-6} to 10^7 cm^{-3} . These instruments have been extensively modified inhouse to provide optimum performance and they are regularly calibrated.

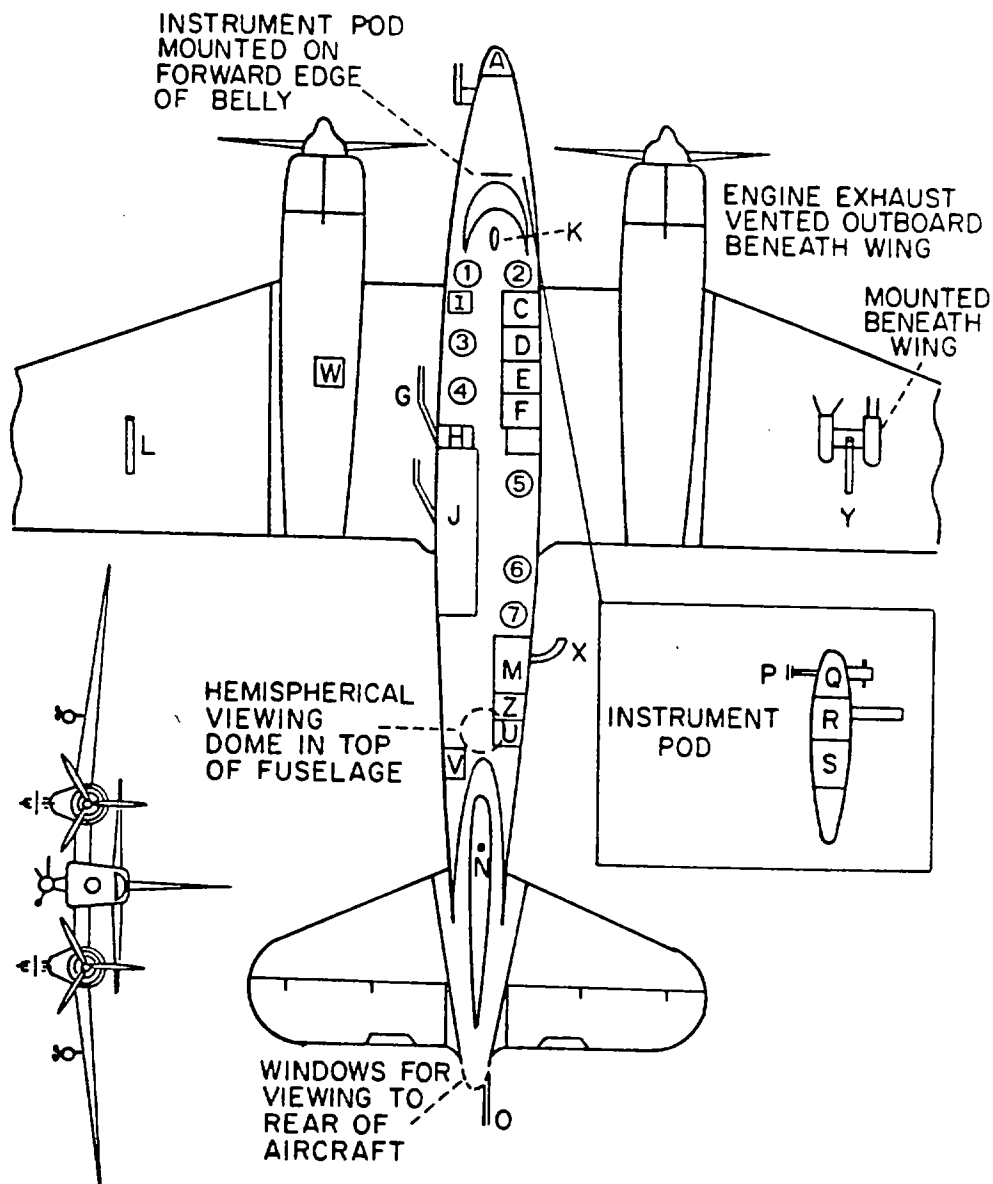
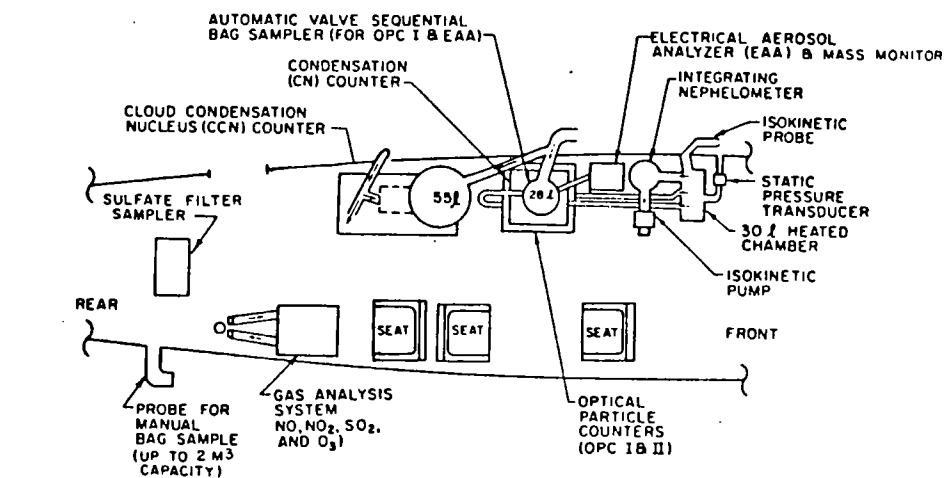


Fig. A.1 Plan view of instrumentation onboard the University of Washington's Douglas B-23 aircraft. Key on following page.

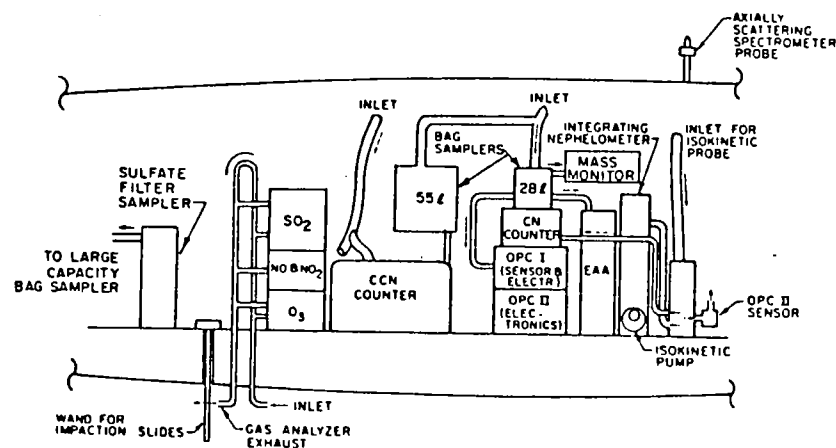
LOCATIONS OF CREW AND RESEARCH INSTRUMENTS ON THE UNIVERSITY OF WASHINGTON'S DOUGLAS B-23 AIRCRAFT

1-2	Pilot and co-pilot	5	Aerosol Instrumentation Monitor
3	Observer	6	Flight Director
4	Instrumentation Engineer	7	Gas Instrumentation Monitor
A	5 cm gyrostabilized weather radar		
B	Rosemount airspeed, pressure altitude and total temperature probes, MRI-turbulence probe and electronics, J-W liquid water probe, angle of attack sensor, vertical gyroscope		
C	VOR-DME slaved position plotter; research power panel (3 KW 110V 60 Hz; 1.5 KW 110V 400 Hz; 150 amps 28V dc)		
D	Electronic controls for J-W liquid water indicator, reverse housing thermometer, electrical cloud particle counter and dew point thermometer, time code generator and time display, WWV time standard receiver, TAS and Ttot analog computers, signal conditioning amplifiers, audio signal mixers, FSK time-share data multiplexers (63 channels), 2-D electric field and turbulence analog read-outs, Doppler horizontal winds		
E	Minicomputer (16 bit word 16k word capacity), computer interface to instrumentation, remote A-D converter, keyboard and printer		
F	Hybrid analog/digital tape recorder (7 track, 1/2") and high speed, 6-channel analog strip chart recorder		
G	Inlet for isokinetic aerosol sampling		
H	Aircraft oxygen, digital readout of all flight parameters, dew point sensor, time code reader and time display, heated aerosol plenum chamber, vertical velocity, Millipore sequential filter system		
I	Controls for metal foil impactor and continuous particle replicator		
J	Aerosol analysis section, generally contains: integrating nephelometer, sodium particle flame photometer, automatic cloud condensation nucleus counter, VHF air-to-ground transceiver, Whitby aerosol analyzer, Royco particle counters, automatic condensation nucleus counter, automatic bag samplers (28 & 55%), mass monitor		
K	PMS axially scattering spectrometer (small droplet probe), vertically mounted		
L	Bomb rack hard point suitable for small instrument pods		
M	Gas analysis system: SO ₂ , O ₃ , NO, NO ₂		
N	Ultraviolet photometer		
O	Electric field mill sensor (vertical and horizontal field)		
P	Reverse flow static temperature probe		
Q	Automatic ice particle counter and metal foil hydrometeor impactor		
R	Continuous Formvar replicator		
S	Tracer ejection pyrotechnic racks (52 40mm units), ion conductivity probe		
T	Engine driven high volume vacuum pump		
U	Radar repeater, side viewing automatic camera, real-time display of PMS data		
V	Radar altimeter, 2-D electric field mill electronics, 20-channel telemetry transmitter		
W	Instrument vacuum system (consists of five high capacity vacuum pumps and one pressure pump connected individually to the cabin)		
X	Anisokinetic large volume aerosol sampler		
Y	PMS optical array precipitation spectrometer. PMS optical array cloud droplet probe		
Z	Sulfate filter sampler		

Key to Figure A.1



(a) PLAN VIEW



(b) SIDE VIEW

Fig. A.2 Details on aerosol and trace gas instrumentation aboard the University of Washington's aircraft.

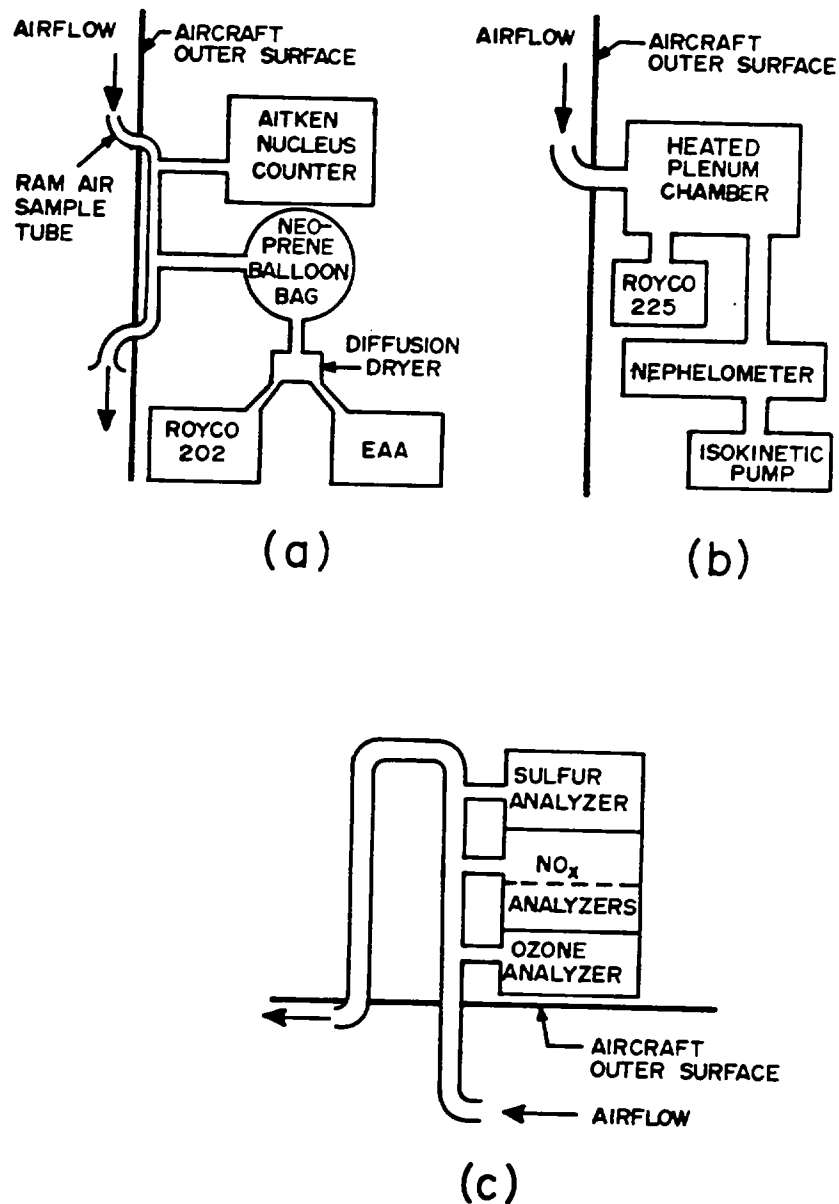


Fig. A.3 Schematic of the air sample inlet system for the (a) Aitken Nucleus Counter, Royco 202 Counter and Electrical Aerosol Analyzer (EAA), (b) Royco 225 Counter and Nephelometer, and (c) Sulfur, NO, NO₂, NO_x, and O₃ gas analyzers.

The sampling system as shown in Fig. A.2 is configured for measuring transient deviations in particles and trace gases (such as those encountered in plumes or clouds). Consequently, air samples are taken in rapidly and automatically by a "grab-bag" sampling system. In addition to the "grab-bag" sampling (which is not completely isokinetic) an isokinetic sampling system is used. Both sampling systems condition the particles to a nearly constant relative humidity (<50%). The plumbing for this system is shown in Fig. A.3.

A general index of the air pollution is obtained using an integrating nephelometer, and automatic condensation (Aitken nucleus) nucleus counter and an oscillating crystal mass monitor.

Since one of the major interests in this study was the effects of the rocket exhausts on the concentrations of cloud condensation nuclei (CCN) and ice nuclei in the air, special efforts were made in this area. Provision was made to supply a diluted sample of the air intakes from the clouds of material produced by the rocket to the automatic CCN counter since the concentrations of CCN were expected to exceed the instrument's range. Also, the NCAR rotating membrane filter was added to provide a time history of the ice nucleus concentration. In addition, a multi-filter manifold was added for measuring ice nuclei by the Millipore filter method using 47mm filters.

A.4 Cloud Physics Instrumentation

The cloud physics instrumentation is designed to provide comprehensive measurements of the sizes, spatial distributions and physical characteristics of solid and liquid cloud and precipitation particles. This information is provided by eight different instruments. Data on solid hydrometeor characteristics (e.g. crystal type, degree of riming and aggregation) are provided by

impaction and Formvar plastic replication. Similar information for millimeter-sized solid and liquid particles is provided by impact markings on the thin metal foil of the foil sampler.

The size spectra (concentration versus maximum particle dimensions) of cloud and precipitation particles over the size range of 3 to 4500 μm are provided by three Particle Measuring Systems (PMS) laser probes. Unlike the impaction devices, the PMS data are processed and displayed in real-time on the aircraft by the computer. Computed values of the effective radar reflectivity and precipitation rate (assuming spherical particles) are also available in real-time.

Cloud liquid water content is measured directly by a hot-wire sensor and is also computed from the PMS data. Ice crystal concentrations are provided by a laser depolarization device developed in this laboratory.

An overall view of the spatial distribution of precipitation is provided by a 5-cm gyro stabilized weather radar.

A complete listing of the instruments aboard the facility for this study is given in Table A.1.

TABLE A.1

SPECIFICATIONS ON RESEARCH INSTRUMENTS ON THE UNIVERSITY OF WASHINGTON'S AIRBORNE ATMOSPHERIC RESEARCH FACILITY

Parameter	Instrument Type	Manufacturer and Model No.	Range	Error	Time Constant	On-Board Recorded?	Power Requirements	Remarks
Total air Temperature (T_{TOT})	Platinum wire resistance	Rosemont Eng. Co. 102CY2CG +414 L Bridge	-100 to +200°C	$\pm 0.1^\circ\text{C}$ (Manuf. Spec.)	≈ 1 sec	Yes	1.4W/28VDC	Modified to give 0-5V output
Static Air Temperature (T_{STAT})	Platinum wire resistance	In House	-100 to +100°C	$\pm 0.5^\circ\text{C}$	≈ 1 sec	Yes	6W/28VDC	Minco resistance element in reverse flow housing (S1088) Recovery coefficient $\approx 0.2-0.3$ Unreliable under icing conditions
Dewpoint	Dew condensation type	Cambridge Model 880	-40 to +50°C	$\pm 1^\circ\text{C}$ (Manuf. Spec.)	2°C/sec	Yes	50W/115VAC	Modified to give 0-5V output for linear output over -40 to +10°C
Pressure Altitude	Absolute capacitance pressure	Rosemont Eng. Co. Model 830 BA	0-15 psi	$\pm 0.2\%$ full scale (Manuf. Spec.)	No specs	Yes	3W/28VDC	
True Air Speed (TAS)	Differential capacitance pressure sensor	Rosemont Eng. Co. Model 831 BA	0- ± 1 psi	$\pm 0.2\%$ full scale (Manuf. Spec.)	No specs	Yes	3W/28VDC	TAS derived by means of on-board in-house built analog computer
Air Turbulence	Differential pressure sensor Model 1120	Meteorology Research Inc.	0-10 $\frac{2}{3}$ cm sec^{-1}	$\pm 10\%$	3 sec	Yes	20W/28VDC	

TABLE A.1 (continued)

Parameter	Instrument Type	Manufacturer and Model No.	Range	Error	Time Constant	On-Board Recorded?	Power Requirements	Remarks
Liquid Water	Hot wire resistance	Johnson Williams	0-2 gm m^{-3} 0-6 gm m^{-3}	No specs	No specs	Yes	110W/115V/400Hz 420W/28VDC	
Electric Field in Vertical Plane	Rotary field mill	Meteorology Research Inc. Model 611	0- $\pm 100 \text{ kV m}^{-1}$	$\pm 10\%$	0.2 sec	Yes	20W/115V/400Hz 120W/28VDC	Modified for 0-5V output and calibration circuitry added for $\pm 20 \text{ kV m}^{-1}$
Hydrometeor Sampler	Metal foil impactor	Meteorology Research Inc. Model 1220A	Particles greater than 250 μm in size				300W/28VDC	
Cloud Particle Sampler	Continuous particle replicator	Meteorology Research Inc. Model 1203D		No specs		Yes	300W/28VDC	
Ice Crystal Counter	Optical polarization technique	In house	0-1000 particles per liter	No specs	Immediate	Yes	180W/28VDC 50W/115V 160Hz	50 μm diameter minimum detected crystal size
Cloud Condensation Nuclei	Optical counting by light scattering	In house	0-5,000 cloud condensation nuclei/ cm^3	$\pm 10\%$	1 Cycle per 15 sec	Yes	500W(Max)/115V/60Hz	

TABLE A.1 (continued)

Parameter	Instrument Type	Manufacturer and Model No.	Range	Error	Time Constant	On-Board Recorded?	Power Requirements	Remarks
Hydrocarbons	Gas chromatograph	Analytical Development Instruments	± 0.1 ppm - 20 ppm (as CH ₄)	50%	variable	Yes	self-contained	Operated to distinguish methane and non-methane hydrocarbons
Ice Nucleus Concentrations	NCAR rotating filter	NCAR	N.A.	No specs	N.A.	No	5W/115V/60Hz	
Altitude above Terrain	Radar altimeter	AN/APN22	0-20,000 ft.	$\pm 5\%$ of indicated value	No specs	Yes	36W/28VDC 120W/115V/400Hz	
Weather Radar	5 cm gyro stabilized	Radio Corp. America AVQ-10	50 nautical miles	No specs		No		Addition monitor at position U
Aircraft Position and Course Plotter	Works off DME and VOR	In house	80 miles	± 1 mile	10 sec	Yes	30W/28VDC	Gives real time plot on sectional map of area of position of aircraft
Time	Time code generator	Systron Donner Model 8220	hrs, min, sec, (IRIG B code)	1 part in 10 ⁵		Yes	12W/115V/60Hz	Modified for 28VDC operation. Hr, min, sec, display

TABLE A.1 (continued)

Parameter	Instrument Type	Manufacturer and Model No.	Range	Error	Time Constant	On-Board Recorded?	Power Requirements	Requirements
Time	Radio WWV	Gertsch RHF 1	min			Yes	1W/28VDC	2.5, 5, 10, 15 mHz Voice announcements are recorded on tape
Ground Communication	FM transceiver	Motorola	approx. 100 miles			No	Internal batteries	150 MHz band
Integrating Nephelometer	Optical Light Scattering	Meteorology Research, Inc. Model 1567	0 to 2.5×10^{-4} 0 to 10×10^{-4}	$\pm 10\%$	10 sec	Yes	200W/115V/60Hz	
Dew Point	Dew condensation type	Cambridge Systems Model TM73-244	-40°C to +40°C	$\pm 1^\circ\text{C}$	2°C/sec	Yes	55W/115VAC/400Hz	Switch selectable ranges for -40° to +10°C and -10° to +40°C
Heading	Gyro-compass	Sperry Model C-2	0-360°	$\pm 2^\circ$	200°/sec	Yes	100W/115VAC/400Hz	Slaved to navigation compass through synero-Digital converter
Ground Speed and Drift Angle	Doppler Navigator	Bendix Model DRA-12	0-20,000 ft.	No specs	No specs	Yes	200W/115VAC/400Hz	Basic sensor for computing horizontal wind direction and velocity.
Ultra-violet Radiation	Barrier-layer photo-electric cell	Eppley Laboratory, Inc. #14042	0-100 $\text{mcal-cm}^{-2} \text{min}^{-1}$	5% full scale	0.1 sec	Yes	1W/28V	

TABLE A.1 (continued)

Parameter	Instrument Type	Manufacturer and Model No.	Range	Error	Time Constant	On-Board Recorded?	Power Requirements	Remarks
Angle of Attack	Potentiometer	Rosemount 861	$\pm 23^\circ$	$\pm 0.5^\circ$	0.1 sec	Yes	1W/28V	
Photographs	35-mm time-lapse camera	Automax Model GS-2D-111	--	--	1 sec to 10 min	--	75W/28V	Automatic recording of time of day, flight number and aircraft heading on each frame.
Total Gaseous Sulfur	FPD flame photometric detector	Meloy 285	0-1 ppm	± 0.5 ppb	0, 1, 10 sec	Yes	200W/115V/60Hz	
Ozone	Chemiluminescence (C_2H_4)	Monitor Labs 8410A	0-5 ppm	± 7 ppb	≥ 1 sec dependent on range	Yes	250W/115V/60Hz	
NO, NO ₂ , NO _x	Chemiluminescence (O_3)	Monitor Labs 8440	0-5 ppm	± 7 ppb	≥ 1 sec dependent on range		200W/115V/60Hz	
Aerosol Particles	Mobility analysis	TSI 3030	1.3×10^{-2} - 4.2×10^{-1} μm	$\frac{1}{\sqrt{N}}$ *			20W/117V/60Hz	
Aerosol Particles	90° light scattering	ROYCO 202 (modified)	0.3-10 μm	$\frac{1}{\sqrt{N}}$			20W/117V/60Hz	

* N = number of measurements

TABLE A.1 (continued)

Parameter	Instrument Type	Manufacturer and Model No.	Range	Error	Time Constant	On-Board Recorded?	Power Requirements	Remarks
Aerosol Particles	Forward light scattering	ROYCO 225 (modified)	1.7-39 μ m	$\frac{1}{\sqrt{N}}$	6 sec [†]	Yes	40W/117V/60Hz	
Aerosol Particles and Cloud Particles	Forward light scattering	PMS ASSP100	2.8-66 μ m	$\frac{1}{\sqrt{N}}$	6 sec [†]	Yes	60W/117V/60 Hz	
Cloud Particles	Diode occultation	PMS OAP-200X	20-300 μ m	$\frac{1}{\sqrt{N}}$	6 sec [†]	Yes	60W/117V/400 Hz 100W/28V DC	
Precipitation Particles	Diode occultation	PMS OAP-200Y	300-4500 μ m	$\frac{1}{\sqrt{N}}$	6 sec [†]	Yes	60W/117V/400 Hz 100W/28V DC	
Aitken Nuclei	Light transmission	General Electric CNC11 (modified)	>0.002 μ m	$\frac{1}{\sqrt{N}}$	1.5 sec	Yes	200/117V/60 Hz	
Aerosol Particles	Direct impaction	Glass slides	5-100 μ m					
Ice Nuclei	Direct impaction	Nucleopore/ Millipore	0.2-200 μ m				150W/28V DC	
Aerosol Particles Mass	Electro-static deposition	TSI Model 3-21	0.2-200 μ m		120 sec	Yes	100W/117V/60 Hz	

[†]Limited by method of recording



APPENDIX B

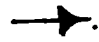
GROUND-REFERENCED AIRCRAFT TRACKS

The coordinates of radar 1.4 are: Latitude $28^{\circ} 29' 34.059''$

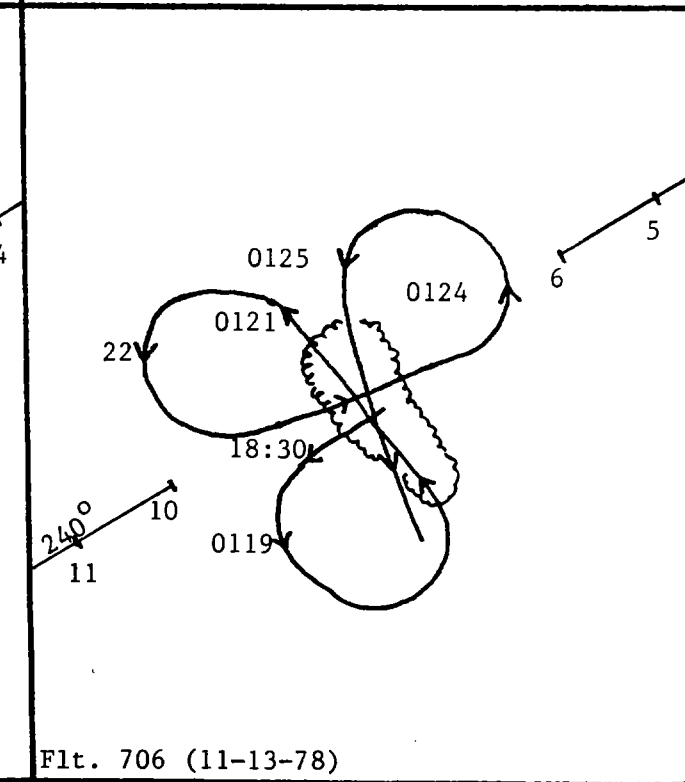
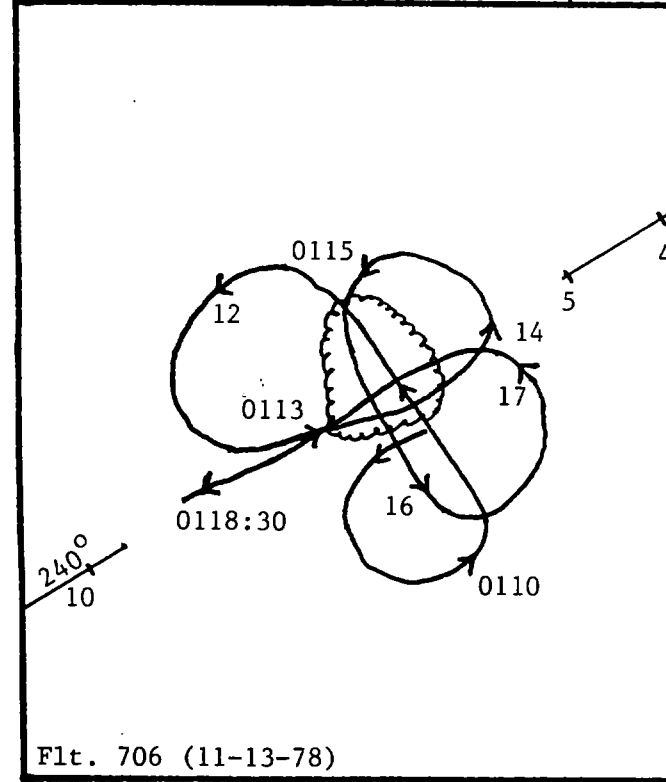
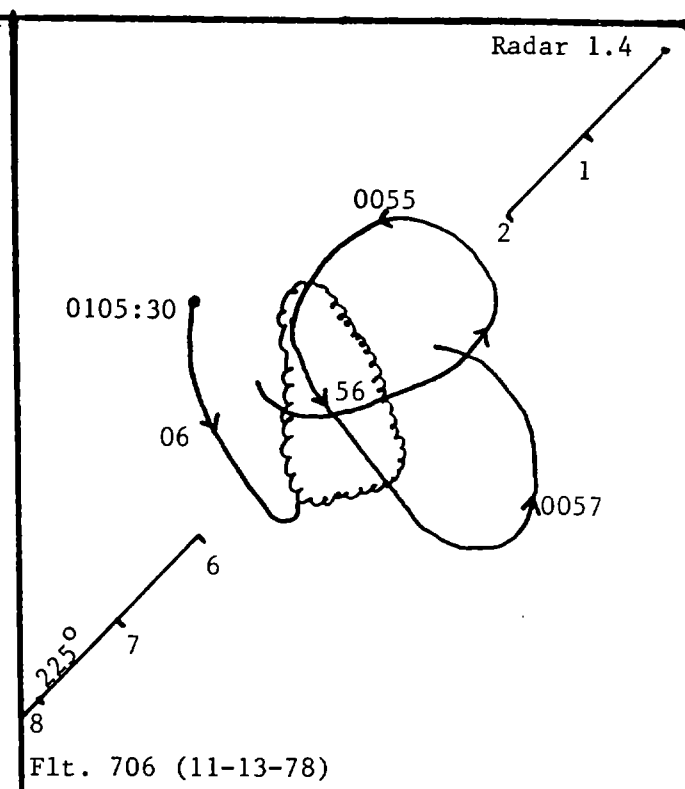
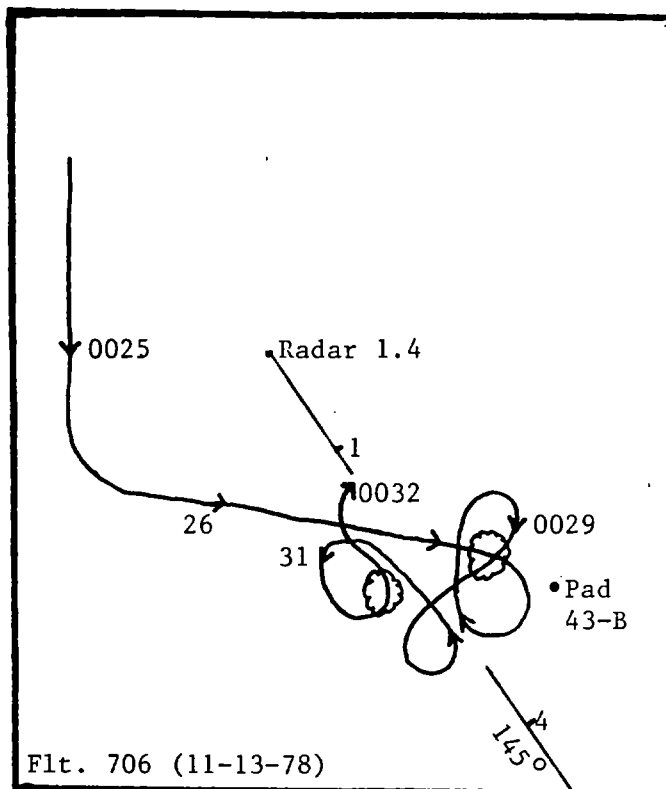
Longitude $80^{\circ} 34' 32.317''$

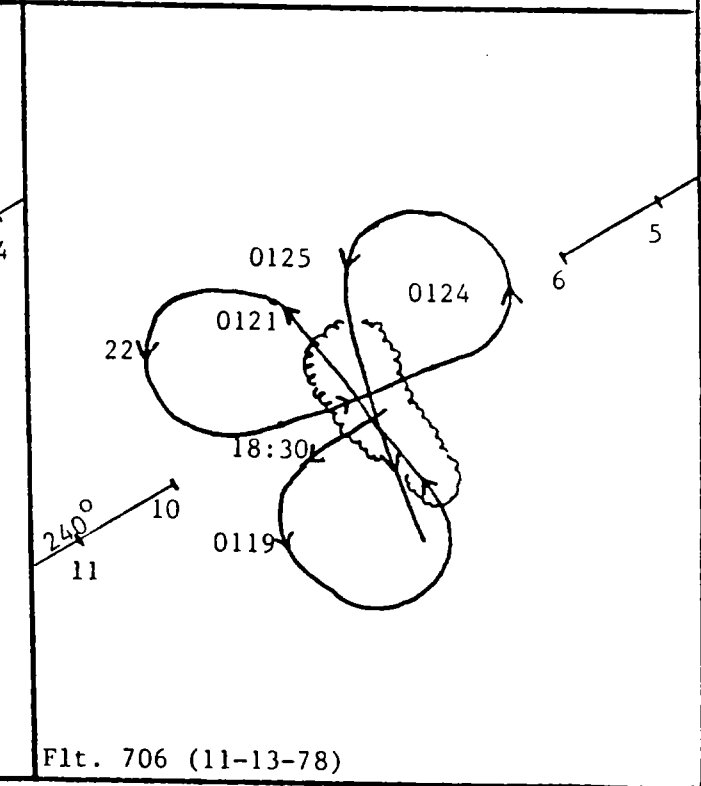
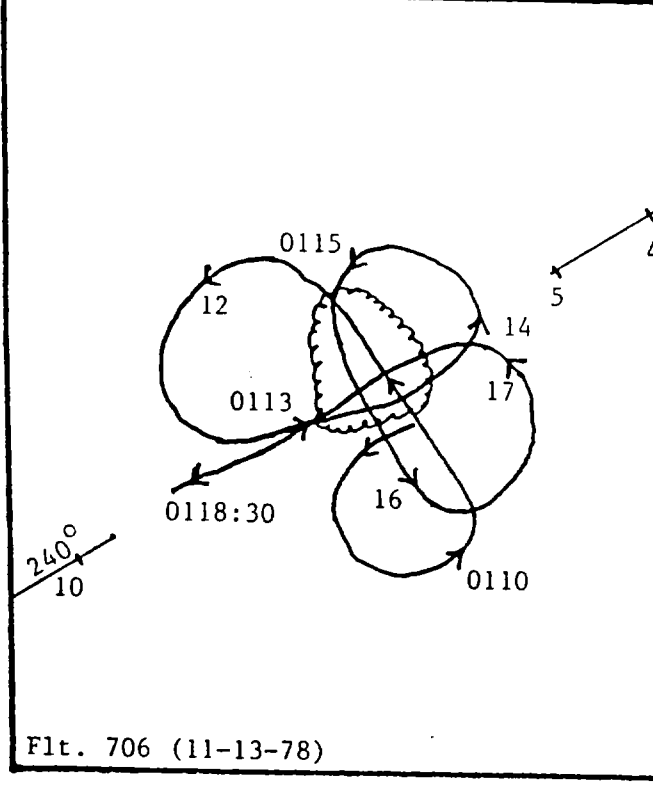
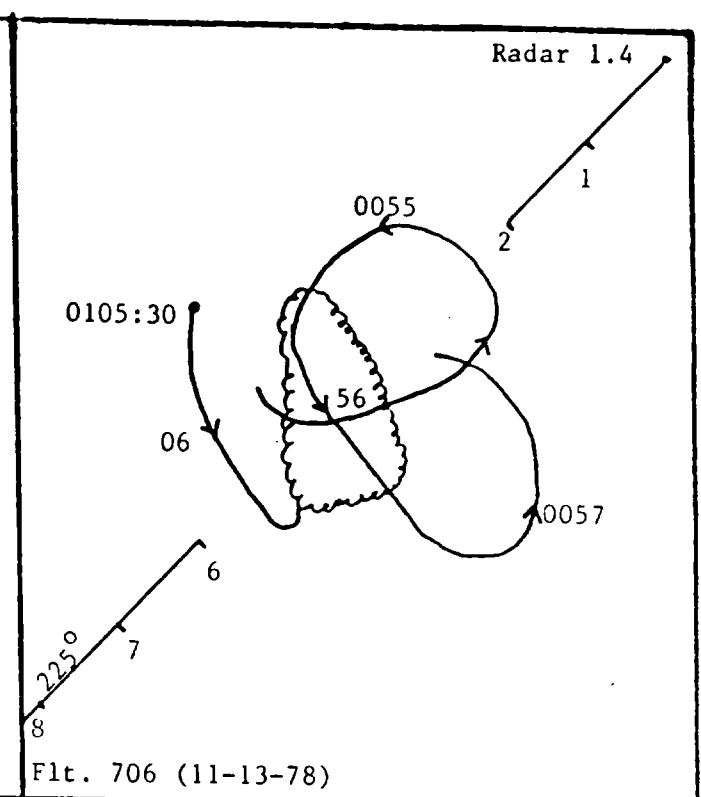
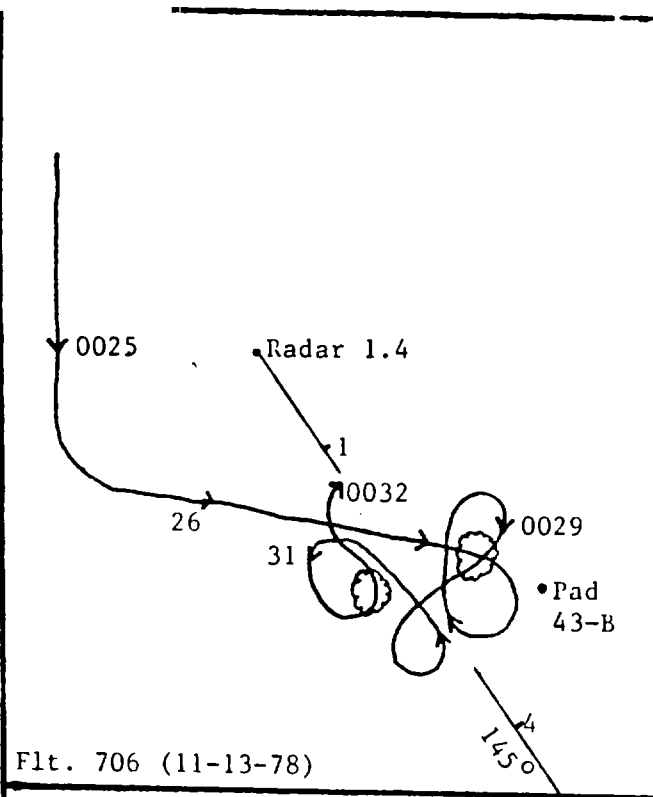
A radial and distance in nautical miles from the radar are indicated on each plot.

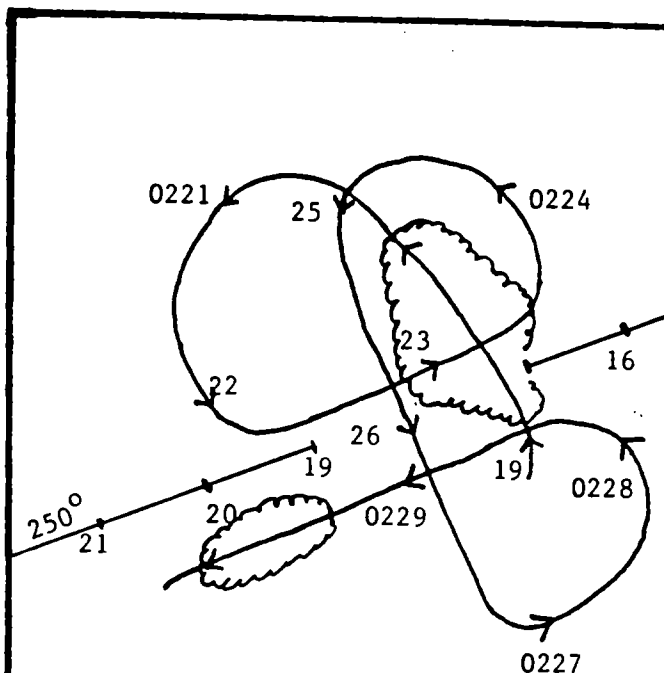
The outline of the ground cloud is indicated by  . If broken,  , the aircraft did not fly through the plume, even though it was in that location on a previous pass.

The direction of movement of the B-23 is indicated by  . The 4-figure numbers on the flight track are the EST in hr and mins.

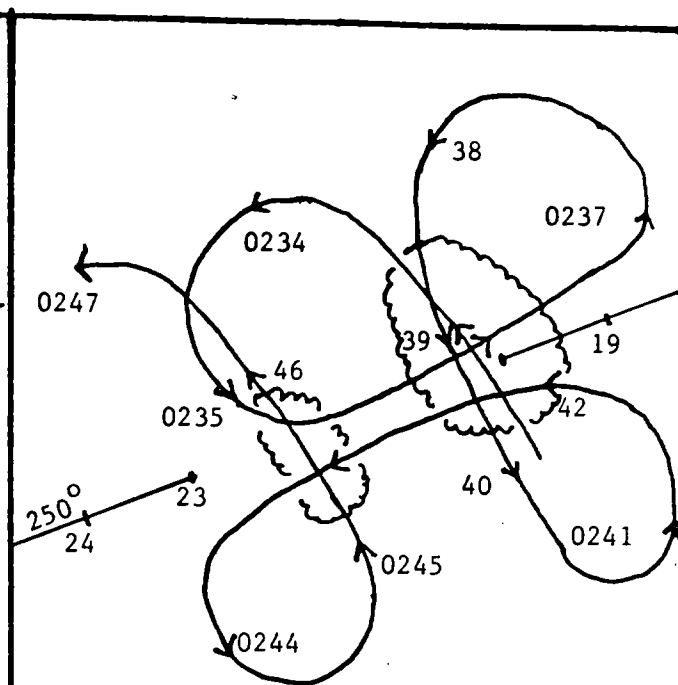
For all but the last plot the scale is 1:125,000. For the last plot the scale is 1:250,000.



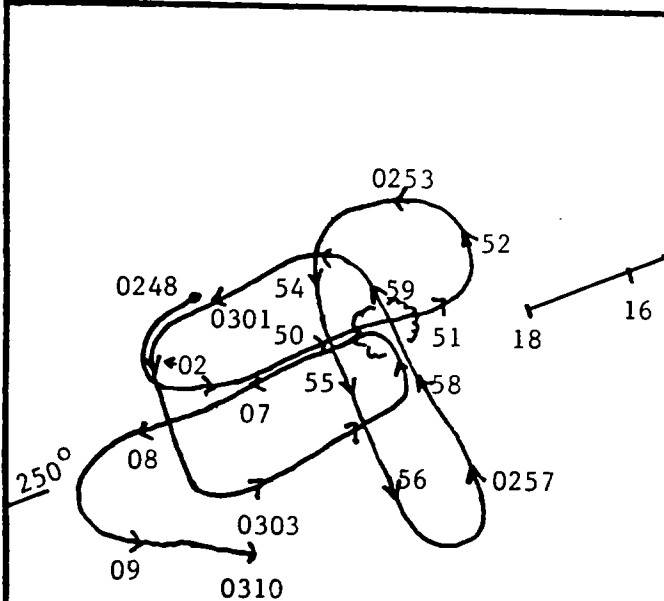




Flt. 706 (11-13-78)

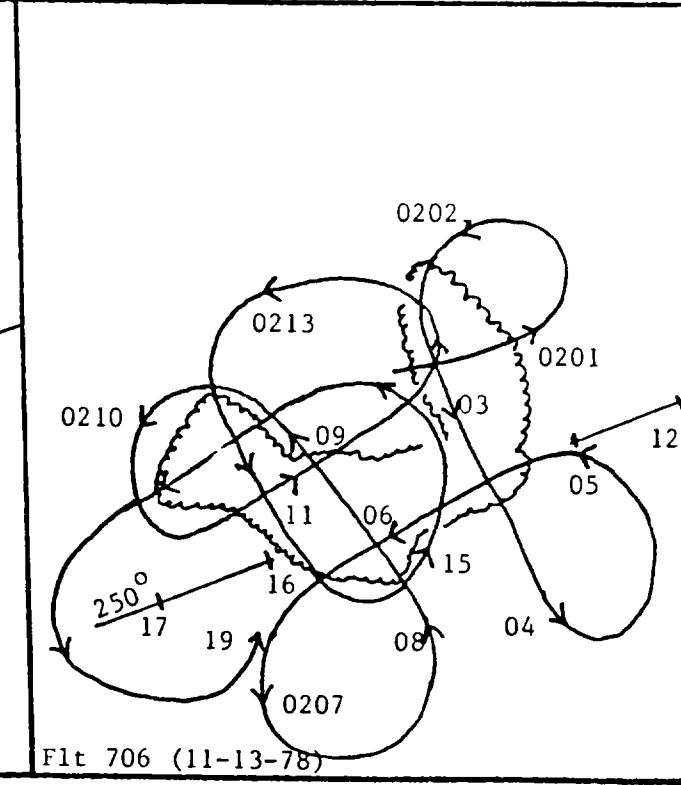
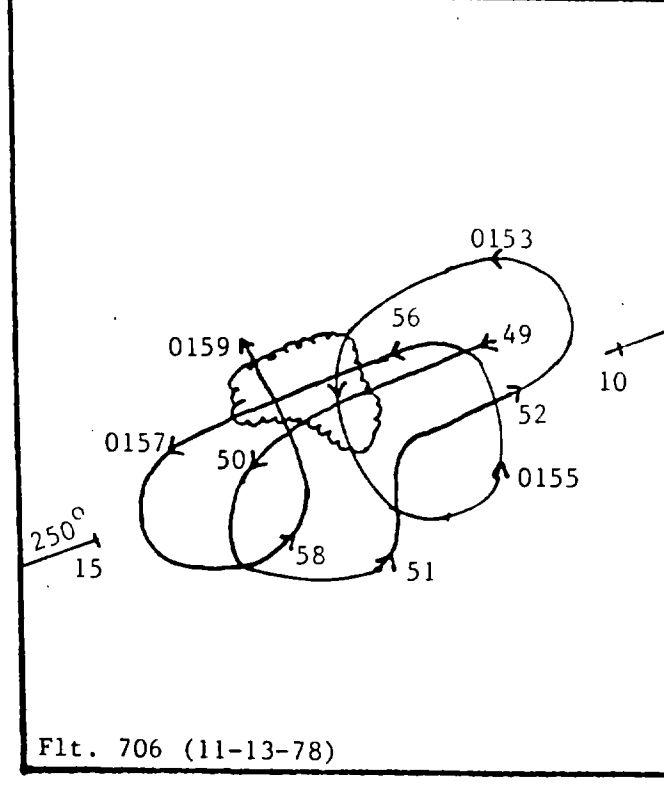
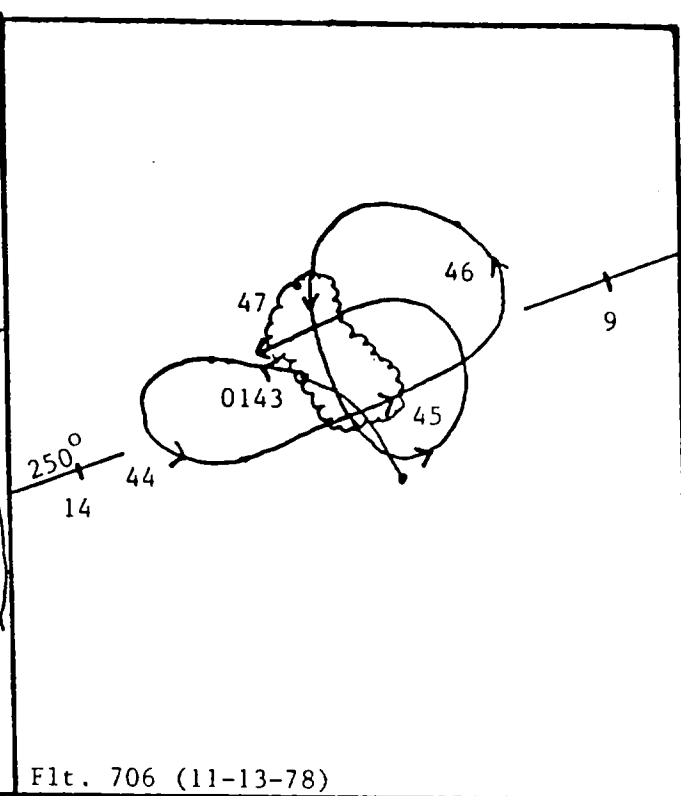
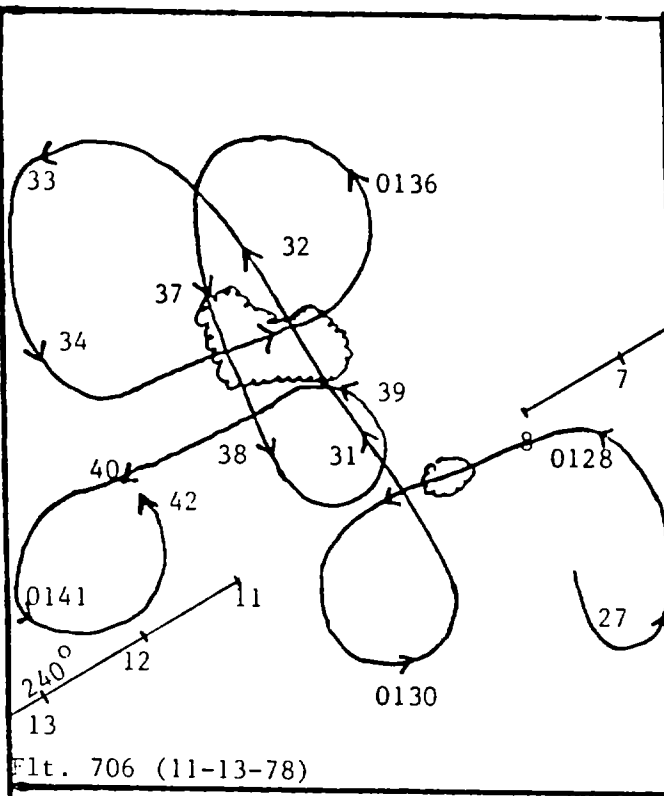


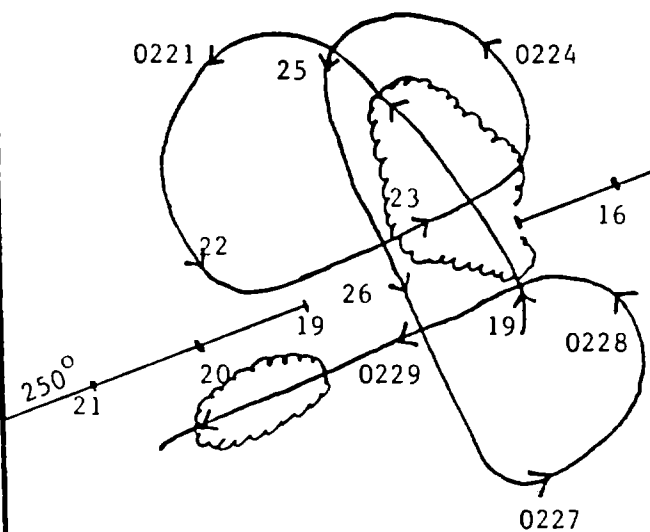
Flt. 706 (11-13-78)



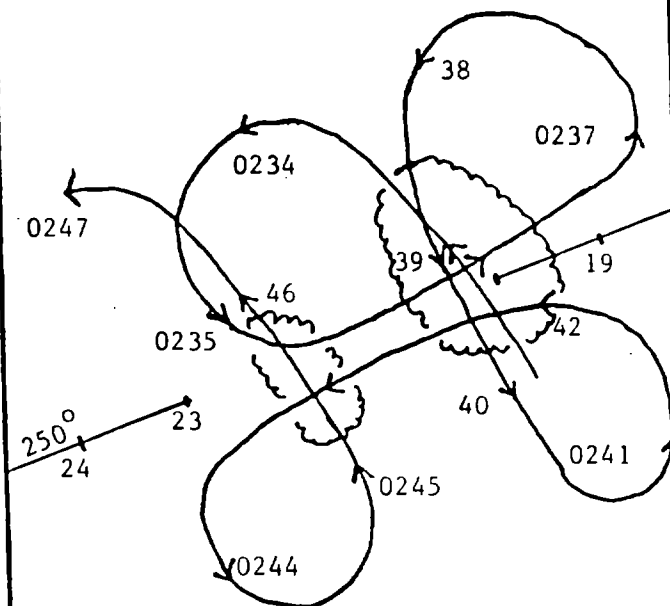
Flt. 706 (11-13-78)

1:250,000

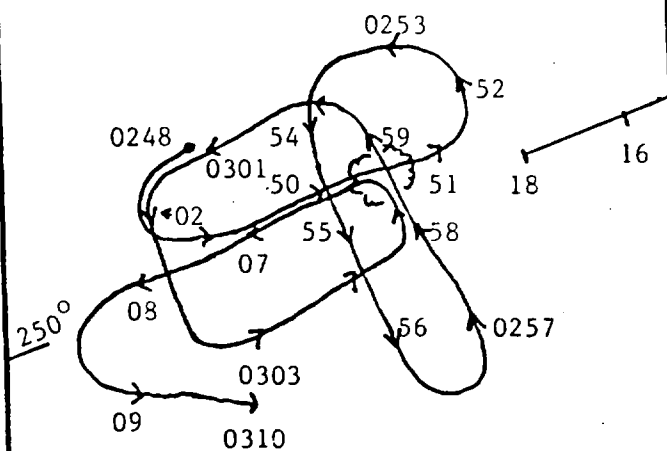




Flt. 706 (11-13-78)

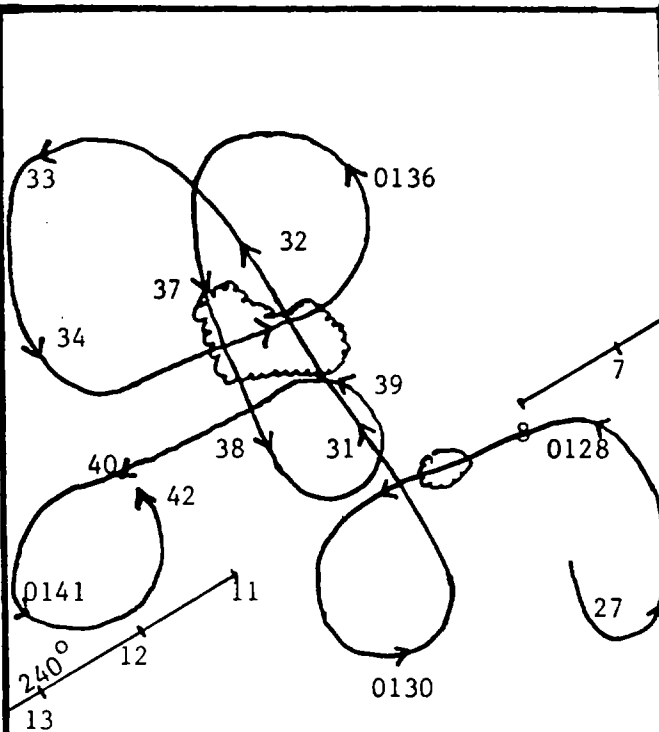


Flt. 706 (11-13-78)

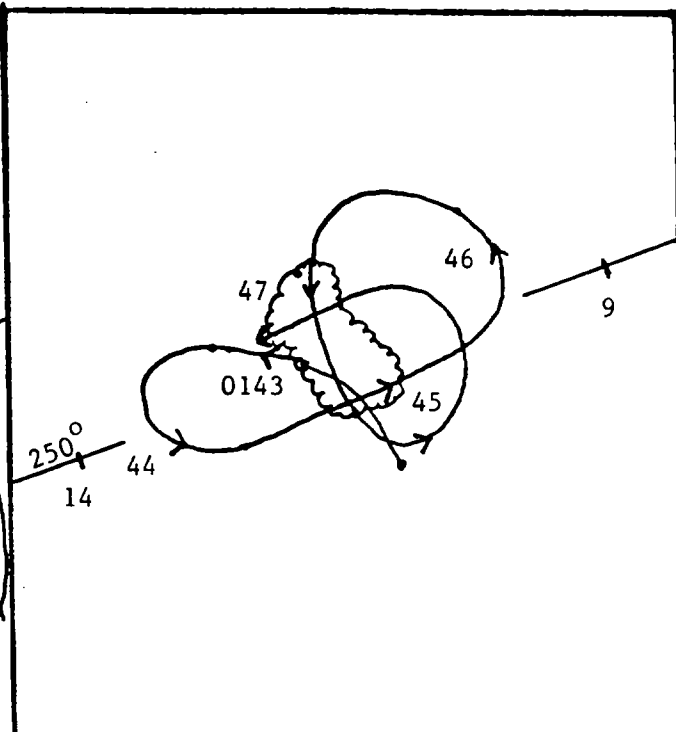


Flt. 706 (11-13-78)

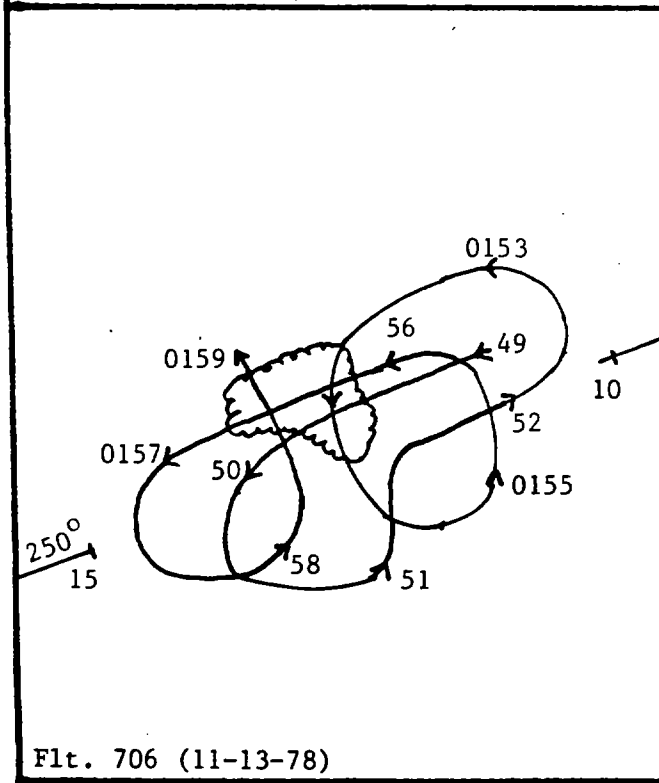
1:250,000



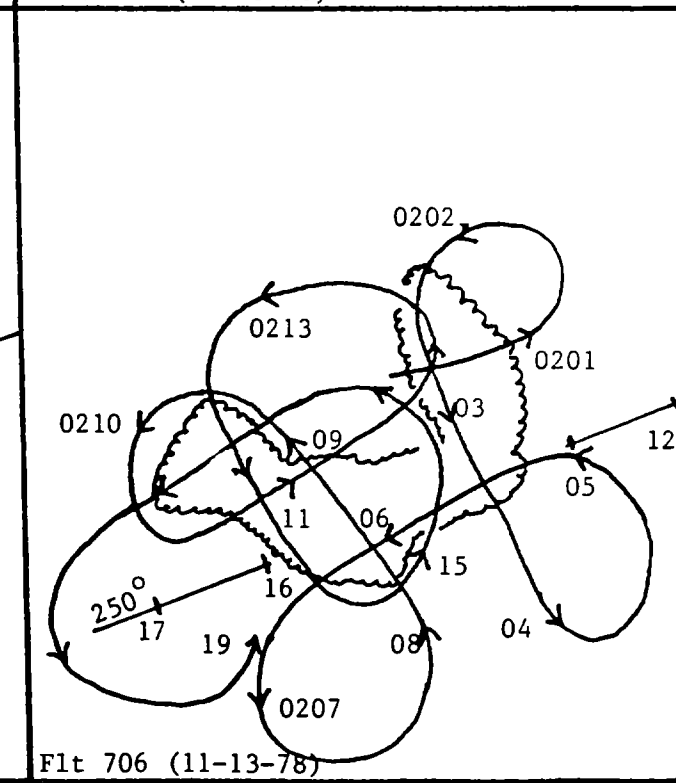
Flt. 706 (11-13-78)



Flt. 706 (11-13-78)



Flt. 706 (11-13-78)



Flt 706 (11-13-78)

APPENDIX C

LIST OF PARAMETERS MEASURED IN THE GROUND CLOUD FOR ALL PENETRATIONS

Shown in Table C.1 are the airborne measurements of state parameters and particle and gas concentrations measured in 52 penetrations of the clouds of material from the Atlas/Centaur rocket. Included in this listing are the dimensions of the ground cloud (2 σ width) for each penetration as determined by the light-scattering coefficient (nephelometer), the width of the region over which there was an ozone deficit, and the excess ion concentration. None of these measurements is a perfect measure of the extent of the ground cloud. The nephelometer has a significant time constant but one which can probably be ignored after $T + 25$ min. The region of ozone deficit is a complex diffusion problem in very stable air and may not represent the dimension of the plume very accurately. The ion concentration meter is an experimental device which has an essentially zero time constant. Therefore, if the region of ions coincides with the ground cloud, this may give the best estimates of the dimension of the cloud for $T + 4$ min to $T + 25$ min. However, our limited experience with this device cautions against its uncritical use. For this reason we do not quote actual values for ion concentration.

TABLE C.1

AIRBORNE MEASUREMENTS IN THE CLOUDS OF EFFLUENTS FROM THE ATLAS/CENTAUR ROCKET

Time (EST)	T _a (°C)	Pressure (mb)	Altitude (m)	Radar Altitude (m)	True Air Speed (m s ⁻¹)	Temp- erature (°C)	Dew Point (°C)	Turbulence (cm ² Sec ⁻¹)	Nephelometer			Ozone			Ion			SO ₂ (ppb)	NO ₂ (ppb)	NO (ppb)	Aerosol Mass (μg m ⁻³)	Aerosol Volume (μm ³ cm ⁻³)
									Cloud Width (m)	Cloud Width (m)	Peak value (x10 ⁻⁴ m ⁻¹)	Cloud Width (m)	Cloud Width (m)	Peak value	Cloud Width (m)	Cloud Width (m)	Peak value					
0028	4	951	521	639	48.1	18.1	1.7	0.2	462	439	1.2	173	16*	40.0	115	109	12	135	195	---	---	
0029	5	957	467	570	40.4	17.3	16.3	1.3	1180	1100	11.6	870	826	4.0	435	413	23	500	635 sat.	---	---	
0030	6	964	404	521	59.7	17.7	16.8	1.2	1122	1065	10.4	1576	1497	2.0	430	408	17	345	505 sat.	324	289	
0031	7	955	485	574	59.9	17.2	16.3	0.2	---	---	---	575	546	4.0	---	---	11	115	140	---	---	
0033	9	951	521	593	58.4	16.8	15.4	---	981	932	8.1	701	666	0.2	350	333	16	330	470	239	232	
0034	10	953	503	597	58.1	16.8	14.4	1.0	1116	1040	7.4	1533	1457	8.0	418	397	15	260	370	---	---	
0035	12	954	494	612	62.0	17.0	15.6	0.1	891	818	4.0	670	636	12.0	223	215	13	140	200	114	100	
0038	14	956	475	581	65.5	16.9	15.6	0.2	679	697	1.2	1572	1493	0.0	---	---	12	40	65	---	---	
0039	15	953	503	577	62.1	16.7	16.0	0.6	1665	1487	2.8	1416	1345	0.0	894	849	9	110	160	134.8	127	
0040	16	957	467	568	57.1	16.9	16.8	0.2	---	---	---	---	---	---	137	130	---	---	---	---	---	
0041	17	950	530	577	58.2	17.8	15.7	0.2	1606	1520	4.4	1257	1194	0.0	1318	1241	9	120	190	---	---	
0042	18	956	475	590	59.7	17.0	16.0	0.3	501	476	1.0	1003	953	12.0	---	---	7	50	70	---	---	
0044	20	955	485	585	60.0	17.0	16.0	0.6	3074	2873	3.2	2140	2052	0.0	1872	1778	9	120	150	---	---	
0046	22	956	575	571	59.4	17.3	16.5	0.3	856	813	2.4	1354	1287	2.0	1140	1063	8	120	180	---	---	
0048	24	958	458	561	60.0	17.2	16.0	0.3	1584	1504	2.4	1728	1642	2.0	1728	1642	8	75	90	---	---	
0050	26	960	440	542	60.9	17.4	16.0	0.4	1680	1527	2.4	1754	1666	4.0	2139	2022	8	60	80	68.6	76	
0051	27	956	475	570	61.5	16.8	16.0	0.2	---	---	---	812	771	26.0	---	---	---	---	---	---	---	
0052	28	956	475	568	62.6	17.1	16.2	0.1	3005	2855	1.8	1803	1713	2.0	2704	2569	7.5	50	50	---	---	
0053	29	959	449	552	62.6	17.2	16.5	0.4	1202	1142	1.8	1953	1855	0.0	2254	2141	8	110	180	---	---	
0054	32	961	431	538	61.9	17.6	16.3	0.5	3045	2893	2.6	3045	2893	1.0	2873	2642	4	80	70	66.9	67	
0059	35	961	431	527	62.7	17.6	16.2	0.1	1354	1287	1.4	2107	2001	4.0	1204	1143	8	55	50	49.1	42	
0101	37	962	422	524	60.7	17.5	16.0	0.3	2185	2076	2.0	1894	1799	0.0	1602	1522	8	50	60	---	---	
0103	39	964	404	517	61.0	17.7	16.1	0.2	1684	1599	1.9	2146	2086	2.0	1903	1808	8	70	110	---	---	
0108	44	963	413	530	60.6	17.4	16.0	0.1	1454	1382	1.8	2400	2280	0.0	1600	1520	8	60	60	48.9	47	
0111	47	960	440	515	60.4	17.3	16.0	0.1	1018	967	1.4	1054	2901	2.0	2618	2497	8	70	110	---	---	
0113	49	965	395	521	61.2	17.6	16.6	0.3	1322	1256	1.6	1616	1535	4.0	---	---	8	50	70	26.9	31	
0115	51	960	440	542	62.3	17.3	15.9	0.1	2593	2548	1.8	2534	2407	1.0	---	---	8	50	65	---	---	
0118	54	961	431	552	64.2	17.4	15.8	0.1	1367	1317	1.0	1464	1391	5.0	---	---	8	40	30	46.3	22	
0120	56	965	395	513	62.7	17.6	16.4	0.2	4364	4166	1.0	4514	4289	0.0	4213	4003	8	60	50	---	---	
0123	59	964	386	510	60.7	17.6	16.4	0.3	2040	1937	0.8	1821	1730	4.0	---	---	8	55	50	22.9	25	
0124:10	64.5	966	386	494	61.7	17.7	16.3	0.1	592	563	0.4	592	563	2.0	---	---	7	40	10	---	---	
0129	65	967	377	481	62.7	17.7	16.3	0.1	---	---	---	603	572	2.8	---	---	7	20	10	---	---	
0132	68	966	386	487	63.7	17.8	16.0	0.1	---	---	---	2217	2106	2.0	2140	2033	7.5	100	115	---	---	
0135	71	966	386	495	63.6	17.9	15.5	0.1	1679	1585	1.0	1603	1521	0.0	2290	2175	8	110	140	43.9	---	
0137	73	965	395	481	63.0	17.7	16.2	0.1	2117	2011	1.6	1814	1724	0.0	2117	2011	8	50	25	18.1	---	
0142	78	968	368	468	62.5	17.8	16.0	0.1	250	232	0.6	2250	2137	4.0	2400	2280	7	40	15	---	---	
0145	81	966	386	482	63.9	17.8	15.9	0.1	1380	1311	1.0	1534	1457	0.0	2070	1967	8	60	70	---	---	
0147	83	965	395	475	62.5	17.7	15.8	0.1	1956	1858	1.2	2182	2073	2.0	3010	2859	8	40	20	30.7	---	
0149	85	965	395	476	63.1	17.7	16.2	0.1	1287	1223	0.8	1363	1295	0.0	1893	1798	8	90	110	---	---	
0154	90	962	422	541	65.1	17.4	15.6	0.2	2343	2226	0.8	2344	2221	4.0	3437	3265	7.5	30	10	---	---	
0156	92	965	395	488	64.4	17.4	15.9	0.2	1855	1762	0.8	2099	1909	1.0	1546	1468	7	30	10	13.4	---	
0203	99	965	395	481	59.7	17.8	15.6	0.1	2579	2459	0.6	3152	2995	20.0	---	---	7	10	10	2.9	---	
0211	109	965	395	471	60.5	17.5	16.2	0.2	2033	1911	0.4	2378	2069	5.0	1049	2897	7	10	10	29.9	---	
0214	110	966	376	484	61.5	17.7	15.8	0.1	3247	3085	0.6	3321	3151	0.0	3542	3365	7	65	45	110	---	
0219:20	115	964	404	485	61.5	17.3	16.3	0.2	4871	4627	0.6	4576	4367	17.0	4289	4066	7.5	25	15	---	---	
0221	119	964	404	478	60.7	17.4	16.3	0.2	2331	2214	0.6	2185	2076	8.0	1184	1115	6	15	15	---	---	
0229	124	965	395	468	61.4	17.3	16.1	0.1	589	560	0.6	1916	1820	14.0	2357	2240	6	10	5	10.4	---	
0236	132	965	395	480	63.1	17.3	16.3	0.2	---	---	---	1483	1399	16.0	---	---	6	10	10	10.1	---	
0239*	135	965	395	481	62.5	17.5	15.6	0.2	1650	1567	0.5	600	520	5.0	600	520	6	60	55	---	---	
0239:30	135:30	964	404	486	62.0	17.5	15.6	0.1	---	---	---	3125	2969	26.0	---	---	6	10	10	---	---	
0250*	146	965	395	481	60.6	17.4	16.0	0.1	---	---	---	1399	1244	22.0	1690	1520	6	25	10	---	---	
0253*	149	961	431	492	63.5	17.1	16.4	0.2	---	---	---	2647	2534	0.0	2010	1860	6	55	40	---	---	
0300*	156	961	431	493	62.5	17.2	15.9	0.1	---	---	---	1875	1741	22.0	2550	2421	5	25	10	---	---	

* Almost certainly an industrial plume.

* Atlas ground cloud probably contaminated by industrial plume.

APPENDIX D

AIRMASS TRAJECTORIES

These air trajectories (Fig. D.1-D.4), which start at Cape Canaveral, are traced backwards in time for a period of 72 hours. They are two-dimensional isobaric trajectories constructed from the observed wind field on the 850 mb pressure surface. All displacements are made parallel to the contours with the distance traveled equal to the product of the 12-hr interval and the mean of the initial and final windspeeds.

This method of trajectory analysis has been shown by Danielson (1961) to be less accurate than an isentropic analysis which incorporates vertical motions and velocity shears into the trajectory computation. However, it was felt that under the synoptic conditions that were present, an isobaric trajectory analysis would indicate the general area from which the air came. The accuracy of these trajectories was verified by comparing them with isobaric trajectories computed on the 700 mb pressure surface for the same time period. The 700 mb trajectories did not differ significantly from the 850 mb trajectories.

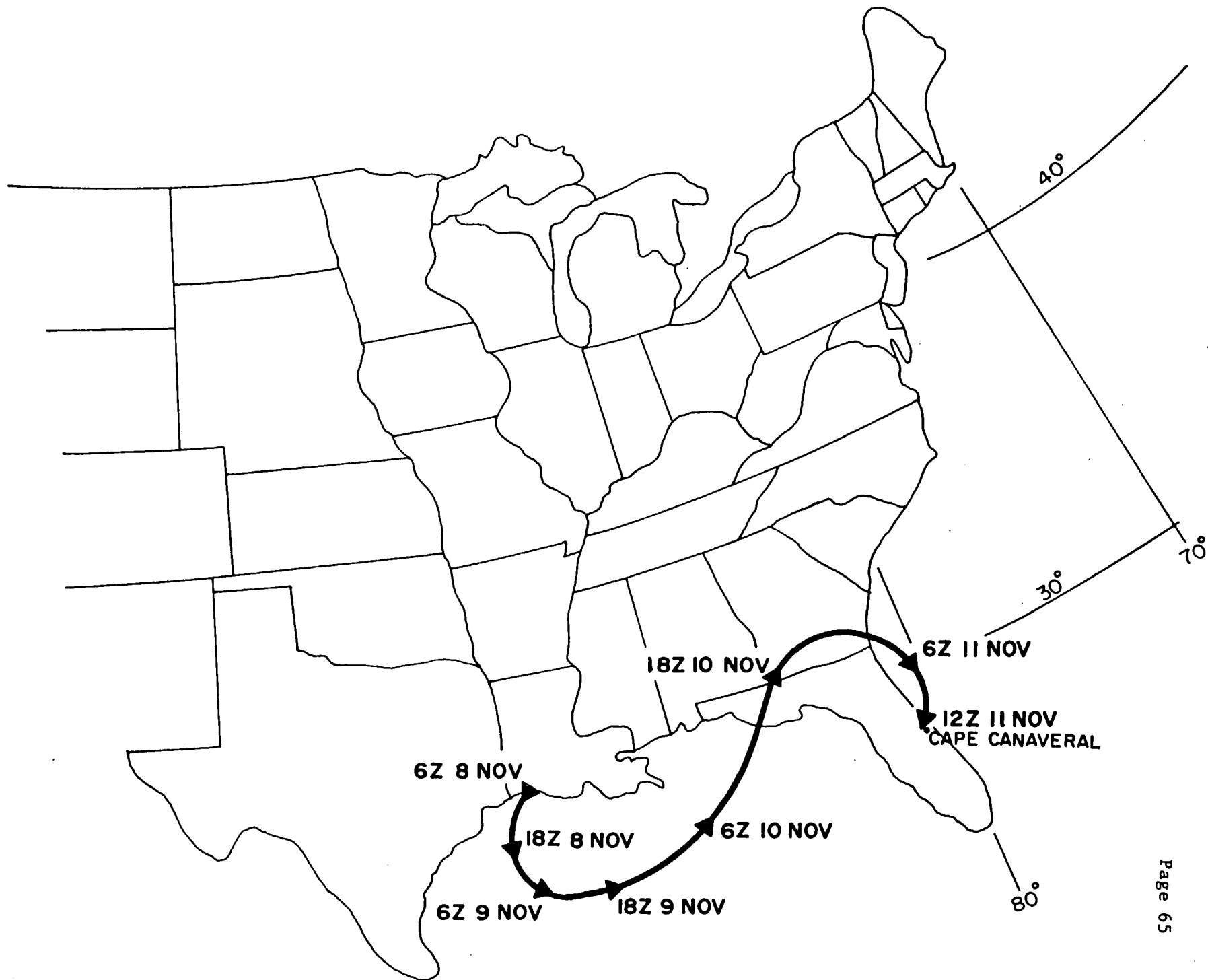


Fig. D.1 Trajectory of airmass that arrived at Cape Canaveral at 1200 Z on November 11, 1978.

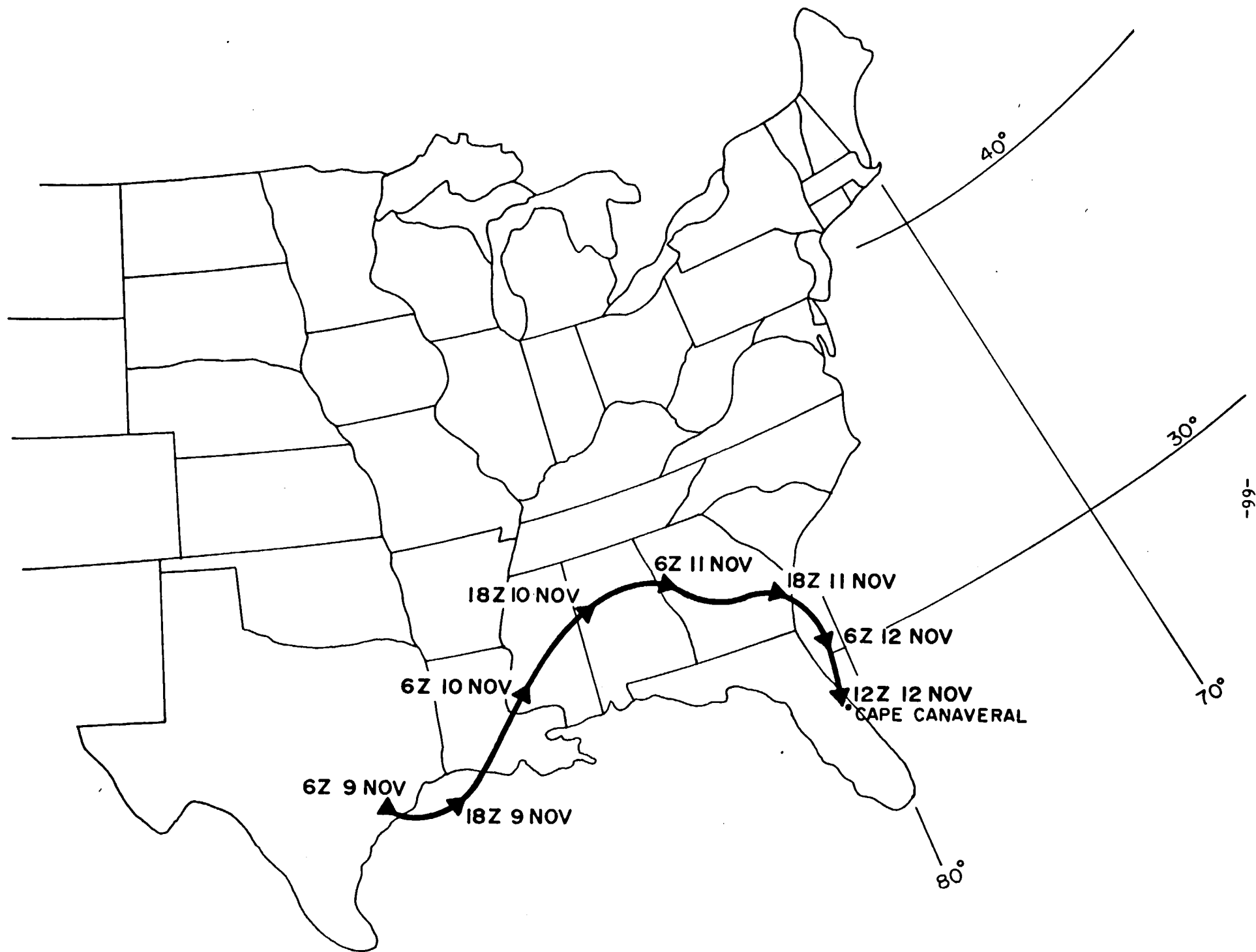


Fig. D.2 Trajectory of airmass that arrived at Cape Canaveral at 1200 Z on November 12, 1978.



Fig. D.3 Trajectory of airmass that arrived at Cape Canaveral at 1200 Z on November 13, 1978.

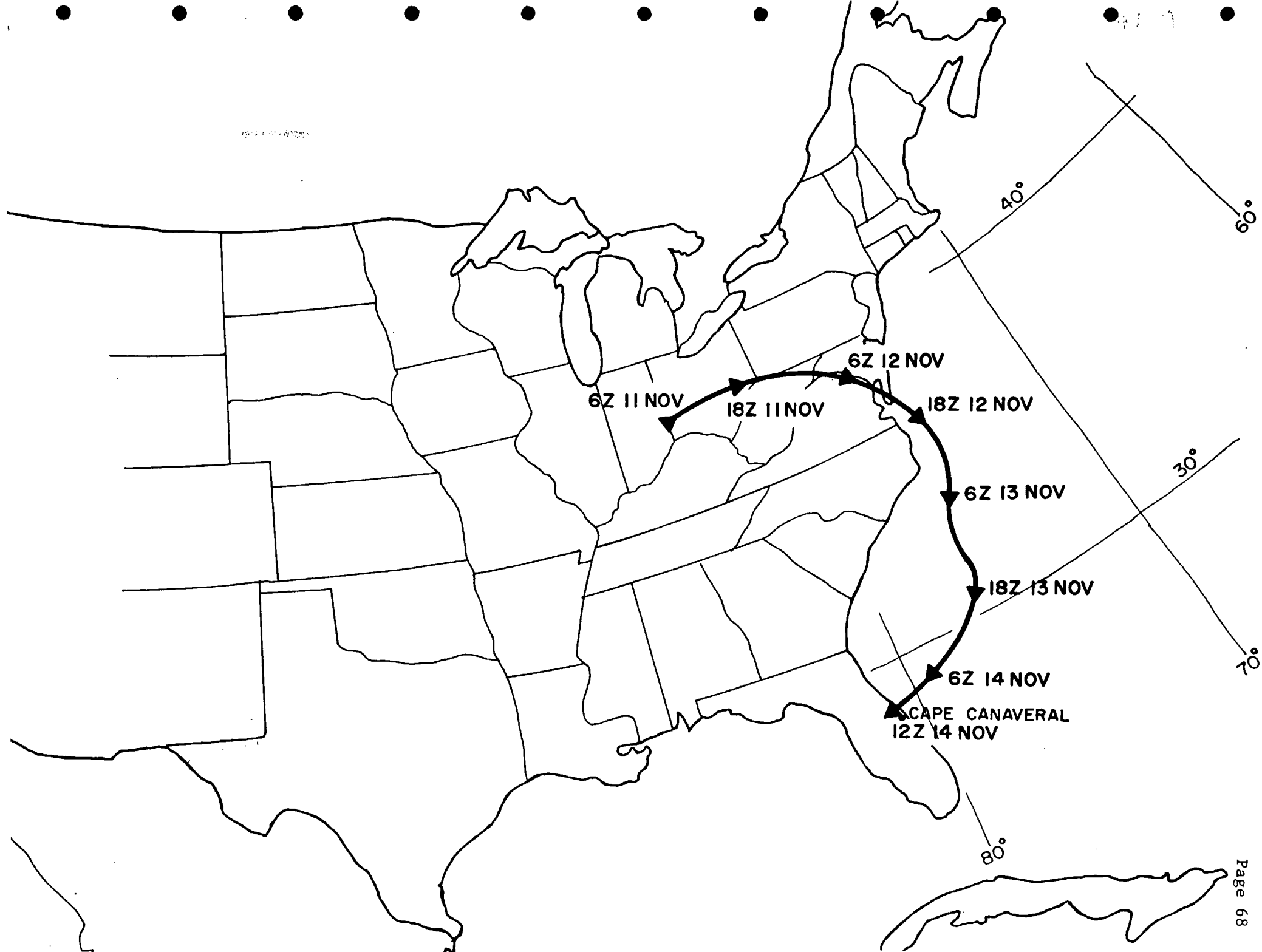


Fig. D.4 Trajectory of airmass that arrived at Cape Canaveral at 1200 Z on November 14, 1978.